FAST EEG BASED BIOMETRICS VIA MEAN CURVE LENGTH

A THESIS SUBMITTED TO
THE GRADUATE SCHOOL OF NATURAL AND APPLIED SCIENCES
OF
MIDDLE EAST TECHNICAL UNIVERSITY

BY

REZA YAHYAEI

IN PARTIAL FULFILLMENT OF THE REQUIREMENTS
FOR
THE DEGREE OF MASTER OF SCIENCE
IN
MEDICAL INFORMATICS

FEBRUARY 2022

Approval of the thesis:

FAST EEG BASED BIOMETRICS VIA MEAN CURVE LENGTH

submitted by **REZA YAHYAEI** in partial fulfillment of the requirements for the degree of **Master of Science** i**n Health Informatics, Middle East Technical University** by,

Prof. Dr. Deniz Zeyrek Bozşahin
Dean, Graduate School of **Informatics** _____

Assoc. Prof. Dr. Yeşim Aydın Son
Head of Department, **Health Informatics** _____

Assoc. Prof. Dr. Tolga Esat Özkurt
Supervisor, **Health Informatics, METU** _____

Examining Committee Members:

Assoc. Prof. Dr. Yeşim Aydın Son
Health Informatics, METU _____

Assoc. Prof. Dr. Tolga Esat Özkurt
Health Informatics, METU _____

Assist. Prof. Dr. Funda Yıldırım
Computer Engineering, Yeditepe University _____

Date: 10.02.2022

I hereby declare that all information in this document has been obtained and presented in accordance with academic rules and ethical conduct. I also declare that, as required by these rules and conduct, I have fully cited and referenced all material and results that are not original to this work.

Name Last name : Reza Yahyaei

Signature :

ABSTRACT

FAST EEG BASED BIOMETRICS VIA MEAN CURVE LENGTH

Yahyaei, Reza
Master of Science, Medical Informatics
Supervisor : Assoc. Prof. Dr. Tolga Esat Özkurt

February 2022, 85 pages

Continuous biometrics using electroencephalography (EEG) has attracted noticeable amount of research for some time. Many state-of-the-art methods have been proposed and achieved satisfactory performances of more than 95 % in recognition rate. In particular, features based on spectral bands and functional connectivity have been preferred for their superior performance. Unlike majority of the previous research, this study chose to focus on the efficiency and ease of implementation. In this direction, we propose a new feature for EEG-based biometrics called the mean curve length (MCL), which is a simple measure of signal complexity based on the Katz fractal dimension. In this study, we evaluated its performance in person identification and authentication, and compared it with other features. For this, a large standard dataset comprising 109 subjects under the eyes-open (EO) and eyes-closed (EC) resting state conditions was utilized. In order to keep the results realistic, minimal preprocessing was performed on the signals, and no subjects or channels were excluded based on their artifacts. A Mahalanobis distance-based classifier was employed for both identification and authentication tasks. For high-dimensional features such as functional connectivity metrics, we used principle component analysis to implement a modified Mahalanobis classifier incorporating

dimensionality reduction. The results of our analyses indicated that MCL provides a remarkably high individual distinction comparable to the commonly preferred features, while being vastly more efficient. Specifically, the recognition accuracies were 99.4 % (EO) and 98.8 % (EC) for identification, and for authentication, the equal error percentages of 6.33 % (EO) and 10.50 % (EC) were obtained. Our study demonstrates MCL as a fast and accurate biometric feature that is promising for real-life and real-time applications. It promotes the effectiveness of nonlinear signal measures in individual discrimination, and encourages to look beyond the conventional time and frequency domain measures of brainwaves.

Keywords: Mean Curve Length, Fractal Dimension, EEG, Biometrics, Mahalanobis Classifier

ÖZ

ORTALAMA EĞRİ UZUNLUĞU KULLANILARAK GERÇEKLEŞTİRİLEN HIZLI EEG TABANLI BİYOMETRİ

Yahyaei, Reza
Yüksek Lisans, Tıp Bilişimi
Tez Yöneticisi: Doç. Dr. Tolga Esat Özkurt

Şubat 2022, 85 sayfa

Elektroensefalografi (EEG) tabanlı biyometri, son zamanlarda ilgi çekici bir araştırma konusu olmuştur. Birçok modern yöntem önerilmiş ve tanıma oranında %95'in üzerinde tatmin edici performanslar elde edilmiştir. Özellikle, spektral bantlara ve fonksiyonel bağlantısallığa dayalı öznitelikler, üstün performansları nedeniyle tercih edilmiştir. Önceki EEG biyometrisi araştırmalarının çoğundan farklı olarak, bu çalışma verimlilik ve uygulama kolaylığına odaklanmayı seçti. Bu doğrultuda, EEG tabanlı biyometri için Katz fraktal boyutuna dayalı basit bir sinyal karmaşıklığı ölçüsü olan ortalama eğri uzunluğu (OEU) adı verilen yeni bir öznitelik öneriyoruz. Bu çalışmada, OEU'nun kişi tanımlama ve kimlik doğrulamadaki performansını değerlendirdik ve diğer özniteliklerle karşılaştırdık. Bunun için, gözler açık (GA) ve gözler kapalı (GK) dinlenme durumu koşulları altında 109 denekten oluşan geniş bir standart veri seti kullanıldı. Sonuçları gerçekçi tutmak için sinyaller üzerinde minimum ön işleme yapıldı ve gürültülere bağlı olarak hiçbir denek veya kanal hariç tutulmadı. Hem tanımlama hem de kimlik doğrulama görevleri için Mahalanobis mesafe tabanlı bir sınıflandırıcı kullanıldı. İşlevsel bağlantısallık ölçütleri gibi yüksek boyutlu öznitelikler için, boyut indirgemesini içeren değiştirilmiş bir Mahalanobis sınıflandırıcısını uygulamak amacıyla temel

bileşen analizi kullandık. Analizlerimizin sonuçları, OEU'nun çok daha verimli olmakla birlikte, yaygın olarak tercih edilen özelliklere kıyasla oldukça yüksek bir bireysel ayrım sağladığını gösterdi. Spesifik olarak, tanıma doğrulukları tanımlama için %99,4 (GA) ve %98,8 (GK) ve kimlik doğrulama için %6,33 (GA) ve %10,50 (GK) eşit hata oranları olarak elde edildi. Çalışmamız, OEU'nun gündelik ve gerçek zamanlı uygulamalar için uygun, hızlı ve doğru bir biyometrik olduğunu göstermektedir. Ayrıca çalışmamız bireye özgü beyin dalgalarının analizinde, geleneksel zaman ve frekans temelli özniteliklerin ötesinde, doğrusal olmayan niteliklerin önemini sergilemiş olmaktadır.

Anahtar Kelimeler: Ortalama Eğri Uzunluğu, Fraktal Boyut, EEG, Biyometri, Mahalanobis Sınıflandırıcı

To Peace

ACKNOWLEDGMENTS

I express my full gratitude to my supervisor Assoc. Prof. Dr. Tolga Esat Özkurt for his complete engagement in my thesis, genuine care about the excellence of my work and all of his support. I am especially grateful to him for allowing me to use the Neurosignal Lab for my work.

I would like to thank Alp Bayar and Kerem Nazlıel for providing remote computing resources and assistance in using them.

The secretary of student affairs in our department, Hakan Güler, has always immediately responded to me whenever I faced any issues in the administrative proceedings during my thesis work. I highly appreciate his exceptional kindness and unconditional helpfulness towards students.

Lastly, I am thankful to my brother, father and mother for their all-time support.

TABLE OF CONTENTS

LIST OF TABLES

LIST OF FIGURES

LIST OF ABBREVIATIONS

AEC	Amplitude Envelope Correlation
AMDF	Average Magnitude Difference Function
AP	Aperiodic Component of PSD
AR	Autoregressive
AUC	Area Under the Curve
BCI	Brain-Computer Interface
CL	Curve Length
CNN	Convolutional Neural Network
COH	Spectral Coherence
COR/CC	Pearson's Correlation Coefficient
CRR	Correct Recognition Rate
DET	Detection Error Trade-off
EC	Eyes Close
EEG	Electroencephalography
EER	Equal Error Rate
EO	Eyes Open
ERP	Event-Related Potential
FAR	False Acceptance Rate
fBm	Fractal Brownian Motion
FC	Functional Connectivity
FD	Fractal Dimension
FIR	Finite Impulse Response
FN	False Negative
FOOOF	Fitting Oscillations and One Over F
FP	False Positive
FRR	False Rejection Rate
Hz	Hertz

IIR	Infinite Impulse Response
KFD	Katz Fractal Dimension
KNN	K Nearest Neighbors
LDA	Linear Discriminant Analysis
LSL	Lab Streaming Layer
MCL	Mean Curve Length
MEG	Magnetoencephalography
MLP	Multi-Layer Perceptron
PLI	Phase-Lag Index
PLV	Phase-Locking Value
PSD	Power Spectral Density
RFE	Recursive Feature Elimination
RMSE	Root Mean Square Error
RNN	Recurrent Neural Network
SNR	Signal to Noise Ratio
SVM	Support Vector Machine
TAR	True Acceptance Rate
TN	True Negative
TP	True Positive
TRR	True Rejection Rate

CHAPTER 1

INTRODUCTION

Human brains contain the most intimate thoughts, memories and feelings of individuals, and hence carry firsthand information of personal identities. This bestows a unique potential capability upon biometrics based on scalp electroencephalography (EEG). Despite many state-of-the-art methods being proposed, EEG-based biometrics is not yet ready to enter the industray. Our study contributes to the ongoing development by proposing a computationally efficient feature, called the mean curve length (MCL), which would crucially benefit the implementation of practical biometric systems based on EEG. In this thesis, we also discuss the factors that affect the performance or hinder EEG from becoming a real-world biometric modality.

Electroencephalograph or EEG is a device that records electrical potentials from the surface of the scalp. These records – called electroencephalogram, which is also abbreviated as EEG – represent the electrical activity of populations of neurons within the brain. To measure the electric potentials, a set of electrodes are placed on the scalp, which, depending on the specific application, can range from 1 to 256 electrodes (Malmivuo, 2012). The electric potential at each electrode is measured in microvolts (μV) relative to the common reference electrode(s). As the electrophysiological fields coming out of the brain are minuscule, electrodes are usually fixed on the scalp using a conductive gel, and the signals are pre-amplified before going into the computer. With the advancement in technology, more user-friendly EEG caps that are dry and portable are being developed (see Section 2.1).

Among the various medical imaging modalities, EEG is characterized by being non-invasive, low-cost and having a high temporal resolution, thus making it applicable beyond the clinical research. In particular, brain-computer interface (BCI) is a major area of technology that utilizes EEG, and EEG-based biometrics may become a potential future technology.

The growing security demands in our vastly interconnected technological world warrants improved methods for identifying and verifying individuals. A good security system for access control must be able to reliably distinguish between an authorized person, trying to access a bank account, building, computer system, server and etc. from an impostor, intending to commit a crime. Traditional means of authorization like passwords, keys, and smart cards no longer meet the requirements of high-security applications. Any people that "possess" these items (e.g., through theft and forgery) are recognized as the authorized individual, regardless of their real identities (Jain et al., 2004). Therefore, it requires for the identifiers of a person to be part of that person. Biometrics is a collection of biological identifiers of a person that can be used in security systems. Fingerprint, face, voice, iris, and DNA are amongst the established biometrics in biometric applications (Gui et al., 2019). Each of the biometrics has its own advantages and weaknesses. Fingerprints and faces are easy to apply, but also easy to forge. There is also a risk of deformation or loss in an unforeseen accident. On the other hand, DNA always exists and does not change, but it is easier to steal, and the process of analyzing it for subject recognition is less practical (Jain et al., 2004).

In recent years, brainwaves acquired through EEG have become a hot topic in the biometrics literature. The reason lies in some peculiar features that EEG has with regard to the other biometric identifiers. Based on the seven criteria defined by Jain et al. (2004) – universality, distinctiveness, permanence, collectability, performance, acceptability and circumvention – EEG brainwaves hold medium to high scores in comparison to the other biometric modalities (Gui et al., 2019) (Table 1.1).

Table 1.1 Comparison between EEG brainwave biometric and other popular biometric modalities. From Gui et al. (2019).

Biometric Identifier	**Universality**	**Uniqueness**	**Permanence**	**Collectability**	**Performance**	**Acceptability**	**Circumvention**
DNA	H	H	H	L	H	L	L
Face	H	L	M	H	L	H	H
Fingerprint	M	H	H	M	H	M	M
Iris	H	H	H	M	H	L	L
Brainwave	H	H	H	M	H	M	H

In this respect, every human possesses a brain that generates brainwaves (universality); contemporary research has shown that the brain activity in every individual has unique features (distinctiveness); EEG is a quantitative measure (collectability); and an optimal recognition accuracy of more than 95 % has already been achieved in numerous EEG biometric studies (performance; Gui et al., 2019). Most importantly, brainwaves are uniquely resistant to circumvention, since they are continuous and sensitive to a person's mental state. In order to obtain a person's EEG, that person must be present, alive and conscious. Thus, it cannot be stolen without one's awareness. Any attempt of coercion will change the person's mental state (e.g., stress and fear) and thus their brainwave patterns (Gui et al., 2019). Synthesizing artificial brainwaves (forgery) is not a straightforward task, although even if someone succeeded in doing so, the previous records can be canceled and replaced by brainwaves elicited under a new mental state or by another stimulus (Gui et al., 2019). This cannot be done for the other biometric modalities.

Until now in five of the seven criteria, EEG exhibits a good potential as a biometric modality. For the two other criteria, namely, acceptability and permanence, substantial research has not been done yet. Since EEG-based biometrics have not yet entered the commercial stage, the willingness of people to accept this new modality is uncertain. And to prove the permanence of EEG characteristics, an extensive timeframe is required to study the robustness of EEG features against time (see Section 5.2). For this, longitudinal multi-session datasets are unfortunately rare.

In the current study, we aim to improve the performance criteria of EEG-based biometrics in terms of computational efficiency. Here we propose MCL, a simple signal measure based on the Katz fractal dimension (KFD) (see Sections 3.3.1 – 3.3.3). It is defined as the average of the absolute value of the first-order difference of a signal, making it one of the most computationally efficient features ever possible to be extracted from EEG signals. We evaluated MCL as a feature for EEG-based biometric identification and authentication on a large dataset. For the purpose of comparison, we also included KFD and some other highly discriminative features

reported in the literature. Mahalanobis distance and a modified implementation for high-dimensional features were employed for classification.

In our methodology, we followed a common framework for constructing a biometric system (Fig. 1.1). EEG signals were first preprocessed by low-pass filtering (Section 3.2). In the next step, features were extracted from the preprocessed signals (Section 3.3). In the user registration stage, these features were stored as templates, along with their covariance matrix, which is required by the Mahalanobis classifier. In the identification or authentication stage, EEG signals of unidentified people went through the same pipeline as in the registration. Their identities were determined in the identification case, or verified in the authentication case, by computing the Mahalanobis distances between their features and the features stored in the database (Section 3.4). We evaluated the performance of our proposed feature using the standard metrics of the evaluation of biometric systems, and compared it with the other features both in terms of biometric recognition performance and computational efficiency (Section 3.5).

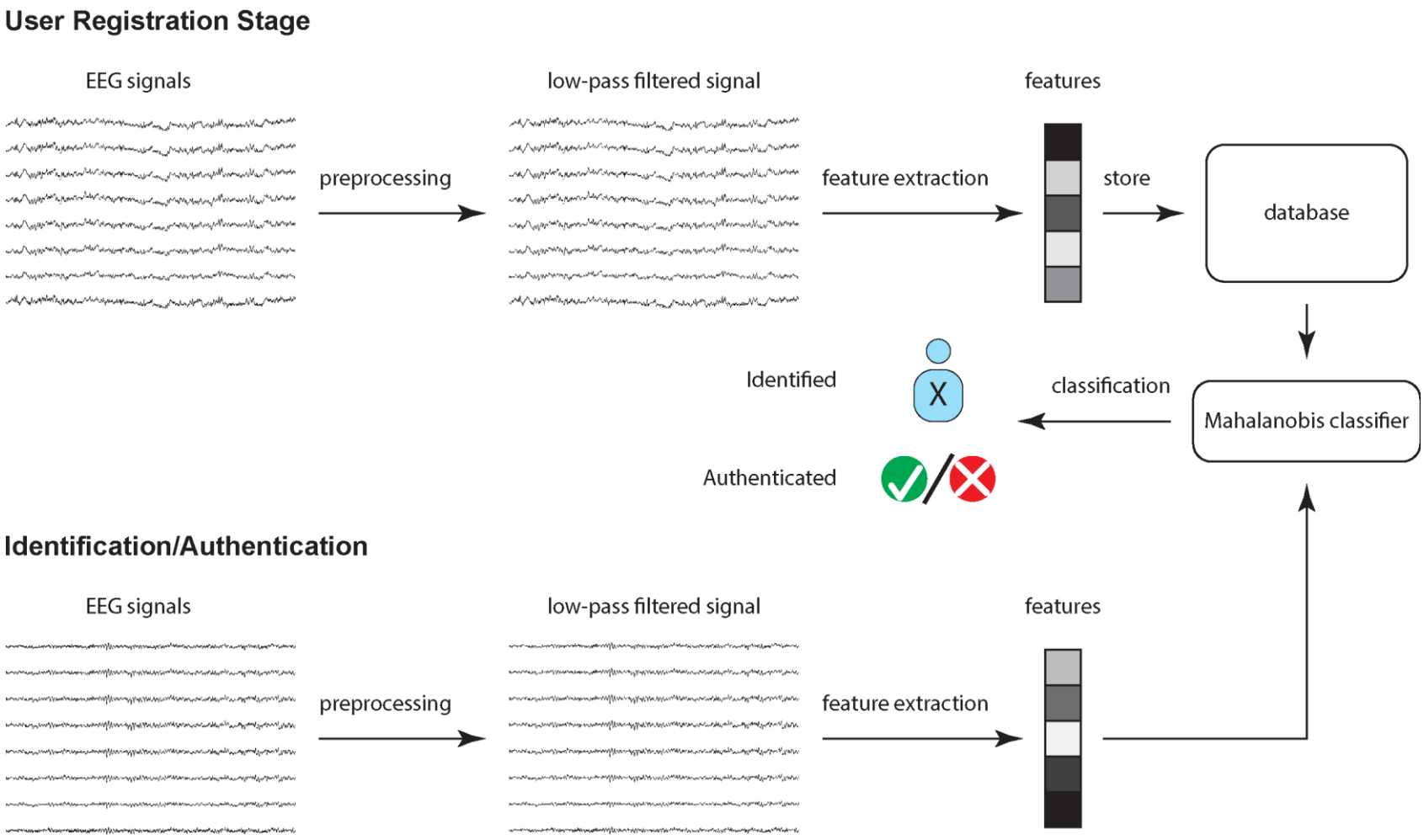

Figure 1.1. Schematic diagram of the biometric system used in this study.

CHAPTER 2

LITERATURE REVIEW

This chapter reviews the concepts and literature that are relevant to our methodology. It starts by reviewing the history of EEG and the current advancements in EEG hardware. Furthermore, it discusses the effects of human mental states and frequency bands on EEG biometric performance. Subsequently, the concept of fractal dimension and other complexity-based measures to which MCL belongs are more extensively reviewed.

2.1 History of EEG and Current Advancements

The history of EEG reviewed in this section is summarized from Millett (2001), followed by the recent advancements in the hardware summarized from Casson (2019).

While the first demonstration of the spontaneous rhythms of the mammalian brain goes back to the 1870s by the English physiologist Richard Caton (1842–1926) and subsequent investigations by many scientists, the development of the non-invasive human electroencephalogram (EEG) can be traced to one man: the German psychiatrist Hans Berger (1873–1941). After his near-death experience after falling off a horse during his military service, Berger received a telegram from his father inquiring about his well-being. He later learned that his older sister had urged their father to contact him, since she felt something terrible had happened to him on the morning of the accident. This seemingly hundred miles away telepathy between him and his sister inspired him to start a life-long career in psychophysics. Berger later followed the works of scientists on mind-brain interaction, the likes of the

experimental psychologist Alfred Lehmann (1858–1921), who theorized that there is a “P-energy” in the brain, which is the psychic energy associated with feelings, emotions and thoughts. For Berger, Lehmann’s energetic model of the brain could provide a physical evidence for rare instances of mental telepathy. Consequently over the next three decades, Berger pursued his investigations based on this model of brain function.

Berger performed his first EEG recording in 1924 during a neurosurgical operation on a 17 year old boy. He removed two Du-Bois-Reymond clay electrodes from an electrical stimulator and attached them to a small Edelmann string galvanometer, a device that had been routinely used for electrocardiogram recordings in the hospital. After weeks of struggle, with large amplifications of the miniscule cortical currents, he could obtain continuous oscillations of the galvanometer string. The first recordings of the human EEG were unimpressive: only short shadowy traces of oscillations captured on a photographic paper (Fig. 2.1). Berger spent his next years trying to improve his new instrument, which he named it *Elektrenkephalogramm* (in German language).

Since Hans Berger, EEG has been continuously evolving. Today, EEG devices are no longer restricted to labs with bulky equipment. They can be wearable and portable, making them practical in real-world applications outside of clinical and lab environments. Other key advantages of EEG compared to other brain imaging techniques are its non-invasiveness and high temporal resolution, which enables it to detect transient brain events. As a result, it is a widely used modality, ranging from diagnostic clinical applications (e.g., epilepsy and sleep disorder diagnosis) to technological brain-computer interfaces (BCI) (e.g., emotional monitoring).

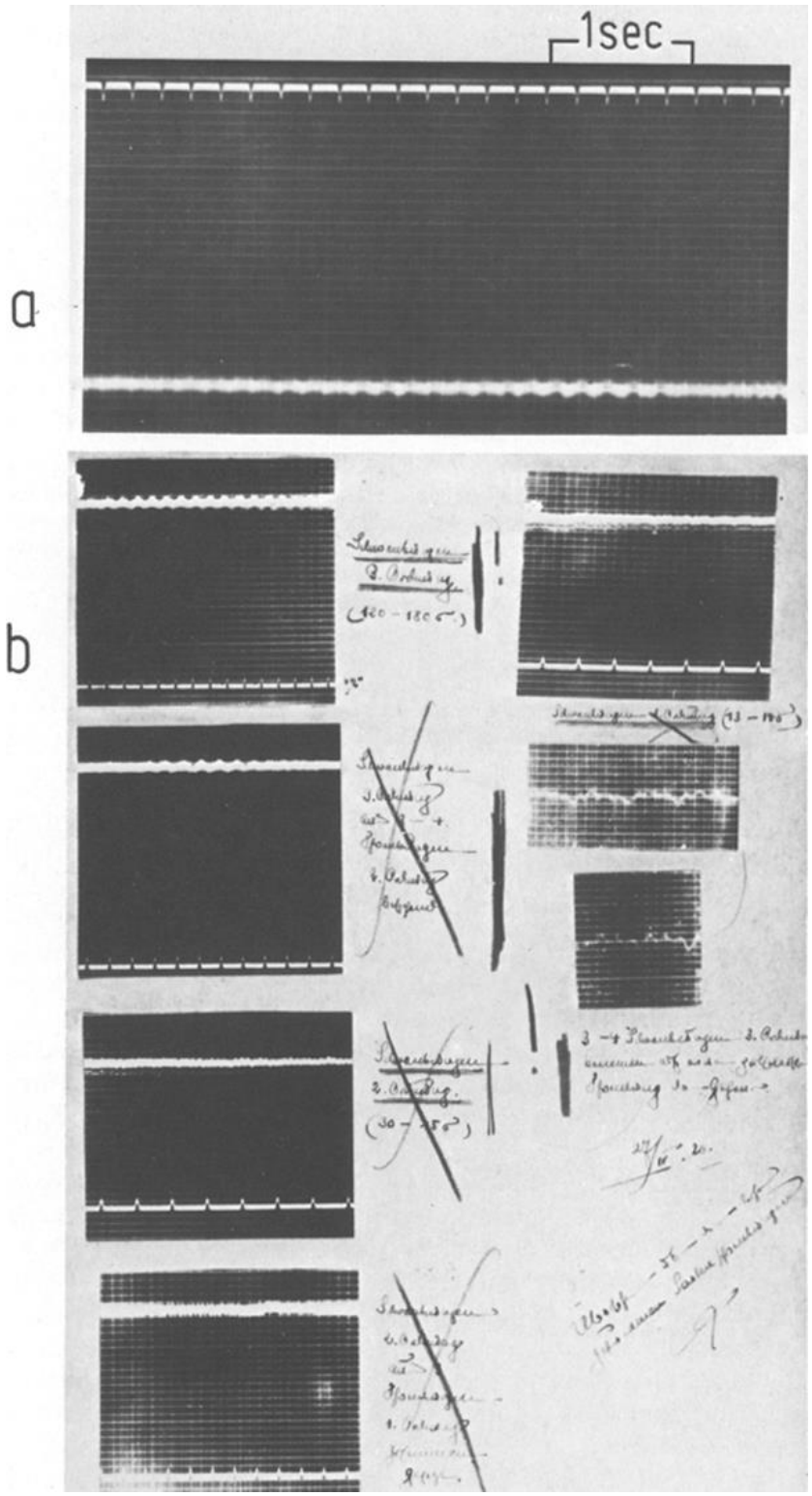

Figure 2.1. One of the earliest electroencephalograms recorded during 1925–1926 by Hans Berger. From Jung and Burger (1979).

The traditional EEG signal acquisition setup that is still preferred in clinical practice and vast majority of research labs use Silver/Silver-Chloride disk-shaped electrodes (Fig. 2.2 (a)), which are connected to a recording instrumentation through long wires (Fig. 2.3). Making a low-impedance connection between the electrodes and the surface of the scalp is essential to properly collect very small biological signals arising from neuronal activity within the brain; hence, usually a conductive gel (e.g., EC2 gel) is applied as a bridge between each electrode and the scalp. However, this gel takes a long time to apply, leaves a mess, is very uncomfortable for the user and requires a trained specialist to set it up. This has prompted research for the development of dry electrodes, which do not require a mediating substance and are easy and quick to set up. A prominent result has been the introduction of fingered electrodes (Fig. 2.2 (b)) that sit on top of the hair and have fingers or prongs to push apart the hair and make contact with the scalp. The drawback of these electrodes compared to the disk-shaped ones is their much smaller contact area, which results in a reduced signal-to-noise-ratio (SNR). Still, there are many other interdependent factors in electrode design which affect the overall performance: materials, manufacturing, attachment methods, electronics and onboard signal processing. With the emergence of 3D printing, it is now possible to create customized EEG electrodes to fit the head shape, hair and skin type and comfort preferences of the user. It also helps to easily perform a wide range of design studies to take into account the interaction of the mentioned factors on the electrode performance.

Nowadays, wearable wireless EEG units are commercially available. They overpass the difficulties in the traditional EEG systems where wires easily get tangled, making them difficult to set up, and unshielded wires are prone to large interferences during motion, due to the electromagnetic induction from 50/60 Hz power grid and other electromagnetic fields present in the environment. Current wearable EEG units have already been tested in out-of-the-lab and motion-rich environments like walking on a treadmill (Gwin et al., 2011; Wagner et al., 2012) and cycling (Kohli & Casson, 2015; Zink et al., 2016), but further improvements are still needed in signal quality and battery life. Limited battery life, which is only hours long at maximum, is the

major shortcoming, and has been traded-off for recording quality. Some proposals for improving the battery life of wireless EEG have been made as the following: using a smaller number of bits for analogue-to-digital signal conversion without significantly impacting the accuracy, improving amplifiers to maintain a low noise floor and wide dynamic range at minimum power consumption, data compression before transmission and other onboard signal processing algorithms to reduce power consumption and improve recording quality.

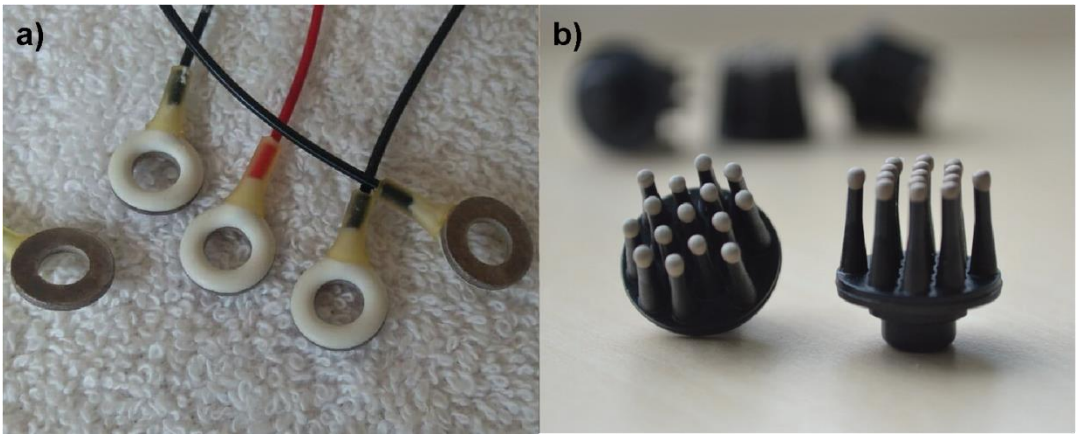

Figure 2.2. (a) Conventional disk-shaped Silver/Silver-Chloride electrodes from Neurosignal Lab, METU Graduate School of Informatics and (b) current fingered dry electrodes from IMEC (n.d.).

Alongside the advancements in EEG hardware, a large number of software toolkits are also emerging to support the development of wearable EEG at the infrastructure level. A major software development to be named is the Lab Streaming Layer (LSL; Boulay et al. (n.d.)) that facilitates synchronization of wearable EEG devices with a wide range of other lab equipment in multi-modal experiments. Built on LSL, SCALA (Blum et al., 2017) is an Android-based app that allows streaming of EEG data to smartphones with real-time analysis.

Figure 2.3. EEG setup with 32 electrodes in laboratory. From Neurosignal Lab, METU Graduate School of Informatics.

Other than wearable EEG devices, there is an emerging focus on beyond-wearable flexible electronics on non-haired regions of the head in order to increase social acceptability. These new sensors collect less information compared to a full head EEG, since they are limited to hairless regions such as the forehead and around ears, but they enable real-world multi-day recordings as well as being socially acceptable.

Finally, there is still a wide range of improvements and innovative possibilities to take EEG out of laboratory environments, and make real-world brain recordings. EEG is probably the only brain imaging modality that can be performed at a low cost in community settings, and hence is increasing its presence in the commercial world, as it becomes more proficient, smaller, easier to set up and socially more acceptable.

2.2 EEG Signal Acquisition Protocols

While recording EEG signals, the mental condition of the subject is an important factor that needs to be considered. Therefore, a signal acquisition protocol for

eliciting a certain brain activity is determined before the beginning of an experiment. EEG protocols are broadly divided into three categories: resting state, stimulus-based and task-based (Bidgoly et al., 2020). Resting state signal acquisition simply refers to recording the brain activity while the subject is at rest either with eyes open or eyes closed. In a stimulus-based protocol, the subject is presented with a visual, auditory, or other sensory stimuli without doing anything. In a task-based protocol, the subject is asked to perform a physical or mental task. Typically for stimulus-based and task-based protocols, the experiments are repeated over many trials and signals are averaged over the trials after being time-locked to an event onset (i.e., the moment when a stimulus is presented or a task is performed; Cohen, 2014). The resulting averaged signal is called an event-related potential (ERP). Since the noise fluctuations are random, they cancel out while averaging, meanwhile the real signal corresponding to the event, which is consistent, is retained in the ERP (Cohen, 2014). Therefore, the signal-to-noise-ratio (SNR) of an ERP is much higher than that of a raw EEG signal.

2.3 Sensitivity of EEG to Human Mental States

While the variation of EEG signals with respect to the change in human mental state is a ground truth, the extent to which it affects biometric performance has only recently come under investigation. For this reason, biometric signal acquisition protocols have been typically restricted to only one mental condition to keep the intra-individual variations in brain activity as low as possible. Two of the studies on EEG task sensitivity are presented in the following.

Yang et al. (2018) employed a dataset recorded from 109 subjects during two resting state and four task-based conditions. They performed experiments in both identification and authentication scenarios by creating training and testing sets with matched and mismatched conditions. They found that while training and testing between different motor movement/imagery tasks did not decidedly affect the

performance, training on the motor movement/imagery tasks and testing on the resting states had a substantial negative effect on the performance.

Wang et al. (2019a) employed the same dataset for a comprehensive study on EEG-based subject identification in diverse human states. They performed subject identification in three different experiments: training and testing the model within each human state, training on resting states and testing on diverse states, and training and testing on diverse states. The highest recognition accuracies were obtained for the identification within each state and slightly less for training and testing on diverse states. The performance noticeably decreased for cross-state identification (e.g., 99.99 % identification accuracy for training and testing on the physical movement data and 85.40 % for training on the resting state data and testing on the physical movement data).

The results from the studies above indicate that at least resting state data cannot be used as a training set for biometric recognition performed under the other conditions and vice versa. Between the choices of resting state and task-based conditions, resting state is mostly preferred in EEG-based biometrics (Gui et al., 2019) for its simplicity and better fit for naturalistic out-of-the-lab environments, where it is difficult to carry out sensory stimulation or mental tasks in a controlled way without special equipment. On the other hand, resting state data are easily affected by environmental noise and artifacts, and thus generally have a lower signal-to-noise ratio (SNR) compared to the brain signals elicited by external stimuli (Bidgoly et al., 2020).

2.4 EEG Time-Frequency Decomposition

Raw EEG measurements reside in the time dimension (with high resolution) and space dimension (with low resolution, defined by the number of electrodes). Often times in EEG analyses, signals are decomposed into different frequency bands (spectral analysis), as they are believed to be associated with different brain functions

(Campisi & La Rocca, 2014). Conventionally, the brain oscillations related to major cognitive processes are divided into five bands, defined by logarithmically increasing center frequencies and frequency widths (Cohen, 2014): delta δ (2–4 Hz), theta θ (4–8 Hz), alpha α (8–12), beta β (12–30 Hz) and gamma γ (30–150 Hz). Please note that there can be minor differences in the exact frequency ranges in different sources.

EEG signals when decomposed into frequency bins of specific resolution include three dimensions: time, frequency and space. Here, the amplitude dimension is excluded, since it is always present in the analyses. Thus, EEG results can be represented in a three-dimensional cube (Fig. 2.4). In general, 1-D and 2-D slices of this cube are displayed in the EEG-related literature (Cohen, 2014).

2.5 Effect of Frequency Bands on Recognition Performance

The frequency band from which features are extracted is an important factor in biometric performance. In the following, the results of some of the studies that have evaluated EEG-based biometrics in different frequency bands are reported.

Thomas and Vinod (2016) performed biometric identification on 109 subjects in the five canonical frequency bands using sample entropy features of resting state EEG. Beta band outperformed the others in both eyes-open (CRR = 98.31 %) and eyes-closed (CRR = 96.94 %) resting state conditions. Moreover, Thomas and Vinod (2018) evaluated biometric authentication by spectral band power features. Their analyses involved three configurations of the resting state data: eyes-open (EO), eyes-closed (EC) and combination of the two. In all configurations gamma band – with EERs of 1.96 %, 1.98 % and 0.8 % in EO, EC and EO & EC, respectively – outperformed the other canonical bands.

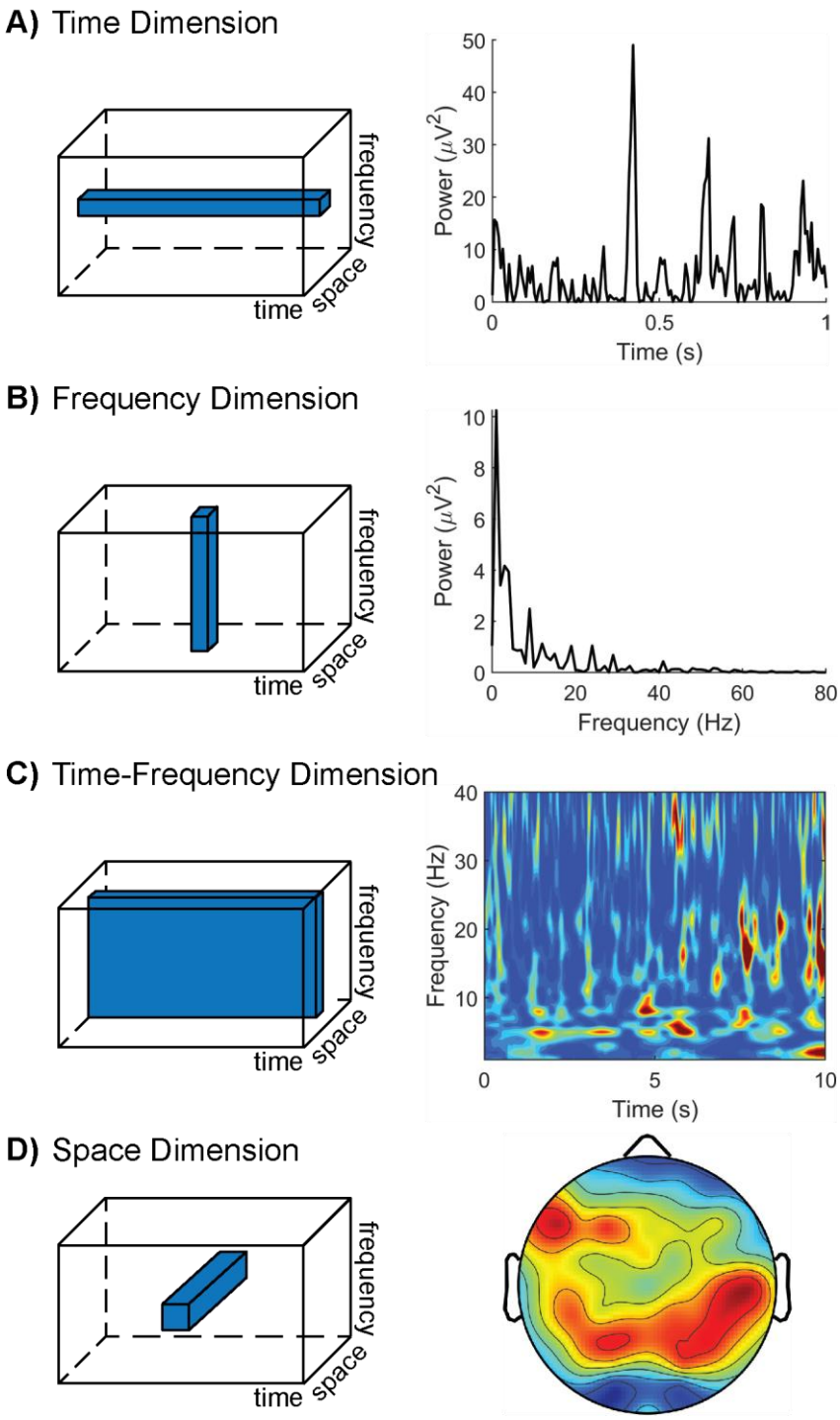

Figure 2.4. Representations of EEG results in different dimensions. From top to bottom: (a) time, (b) frequency, (c) time-frequency and (d) topographical representations. For (c) and (d), the amplitude dimension is color coded. Adapted from Cohen (2014).

Kong et al. (2019) performed biometric identification using PLV features in four frequency bands (excluding delta band). The study employed three datasets, recorded from 20, 12 and 9 subjects during performing various tasks, and the best identification accuracies were obtained for beta band (CRR = 98.1 %), gamma band (CRR = 98.9 %) and beta band (CRR = 99.6 %), respectively.

Fraschini et al. (2018) performed biometric authentication in six frequency bands, where beta band was further divided into low-beta (13–20 Hz) and high-beta (20–30 Hz). The following functional connectivity metrics were evaluated on two datasets, obtained from 109 (DS1) and 11 (DS2) subjects in EC condition: correlation coefficient (CC), phase-lag index (PLI), amplitude envelope correlation (AEC) and phase-locking value (PLV). The best frequency band results in DS1 and DS2 were high-beta band for CC (EER = 6.63 % and 12.91 %) and gamma band for PLI (EER = 5.70 % and 11.65 %), AEC (EER = 13.86 % and 17.31 %) and PLV (EER = 5.91 % and 3.07 %).

Wang et al. (2019a) performed biometric identification using PLV features in the five frequency bands. Two datasets obtained from 109 and 59 subjects were employed for the study, both consisting of two resting state (EO and EC) and two task-based conditions, where the types of the tasks were different for the two datasets. They found that beta and gamma bands yielded better identification accuracies, regardless of the types of classifiers or human states being used. Wang et al. (2020) extended the previous study to various brain networks, where all combinations of twelve different graph measures (e.g., nodal degree) extracted from the brain networks built by six different connectivity measures (e.g., PLV) were evaluated. Once again, either beta or gamma band, depending on the measures and dataset used, facilitated better performances.

da Silva Castanheira et al. (2021) performed biometric identification with spectral and connectome features using broadband as well as bandlimited magnetoencephalography (MEG) signals collected from 158 subjects. Spectral features performed best (CRR = 97.5 %) in high-gamma band (50–150 Hz),

identically in broadband, beta and gamma bands (CRR = 96.2 %), and slightly less in the lower frequency bands of delta (CRR = 94.9 %), theta (CRR = 95.6 %) and alpha (CRR = 95.6 %). Connectome features performed best in beta and theta bands (CRR = 100 %), slightly lower in alpha (CRR = 99.4 %), gamma and delta bands (CRR = 98.7 %), and worst in high-gamma and broadband (CRR = 94.9 %).

The studies above span variety of features, conditions and datasets for EEG-based (and MEG-based) subject identification and authentication. The general trend is that higher frequencies, beta and gamma bands in particular, seem to contain the most discriminating information about individuals. Different features perform best in different bands and even the particular dataset can affect the relative results.

Nevertheless, according to Fraschini et al. (2014), the better performance in higher frequencies should be interpreted with caution. It is suggested that the characteristic higher frequency activity might be stemming from muscle artifacts, as they mainly contaminate the higher frequency range (20–80 Hz with a peak around 40 Hz) (Malafeev, 2018) and vary considerably across individuals (Goncharova et al., 2003). Hence, they may be partially responsible for increasing the discrimination performance. It is difficult to estimate to what extent these non-representative components contaminate the signals from brain sources. Nonetheless, Fraschini et al. (2014) presented two possible ways to empirically confirm their existence: first by using longitudinal datasets, assuming that these muscle artifacts vary across acquisition sessions. The other way is to collect signals using MEG, which is less susceptible to contamination from muscle activity (Claus et al., 2012). However, the latter did not have a decisive effect on the results of da Silva Castanheira et al. (2021).

2.6 Fractals and Fractal Dimension

The concept of fractals and fractal dimension was introduced by Benoit B. Mandelbrot (1924–2010) in his 1967 paper, “How long is the coast of Britain?” (Mandelbrot, 1967). He noted that measuring geographical curves with a

conventional notion of length is meaningless, as the measured quantity can increase indefinitely by decreasing the length of the "ruler" used to trace the curve. This is because when using smaller rulers, lengths of smaller details are added to the total length. Moreover, when zoomed in, these small details look like a reduced-scale version of the whole curve, which gives such curves a property of "self-similarity" (Fig. 2.5). How much new details emerge while a curve is scaled-up is related to the degree of complexity of the curve. For self-similar curves, the level of complexity is quantified by "an exponent of similarity, *D*, which possesses many properties of a dimension" (Mandelbrot, 1967), although it is usually a fractional number between 1 and 2. This is in contrast to the conventional notion of curves being one-dimensional geometrical shapes. The fractal dimension is an alternative way to compare between fractal shapes (such as geographical curves) for which the conventional measure of length is undefinable.

Fractal dimension quantifies the rate of increase in a geometrical object's observable details as it is zoomed in. Mandelbrot (1967) defined it by generalizing the concept of dimension for the familiar integer dimensions: a straight line has a dimension of one, since scaling it up by a factor of N yields a line containing $C(N) = N$ exact copies of the original size line (Fig. 2.6). A square has a dimension of two, since scaling it up along each of its sides by a factor of N yields a greater square that exactly contains $C(N) = N^2$ copies of the original square. Similarly, a cube with a dimension of three would contain $C(N) = N^3$ copies of itself when scaled up. In general, a D-dimensional object enlarges by a factor of $C(N) = N^D$ when scaled up by a factor of N along each side. Thus, the dimension D is defined by the relation $D = \log C(N) / \log N$.

Figure 2.5. West coast of Britain (left) and a scaled up section of it (right). Geographical curves are some of the natural phenomena that exhibit self-similarity at different scales.

How the above relation can be used to find the fractal dimension of a structure, is demonstrated following an example from Pilgrim and Taylor (2018) on a simple mathematical fractal object by the name of Koch curve (Fig. 2.7). It is constructed as follows: beginning with a straight line, the middle third of the line is removed and replaced by two sides of an equilateral triangle whose side is 1/3 of the initial line. The resulting shape is thus made out of four new line segments of 1/3 length of the previous line. This process is iteratively repeated for each of the new lines, adding finer details in each iteration (Fig. 2.7). As the number of iterations goes towards infinity, the resulting curve tends towards a "strictly" self-similar object, which can be decomposed into parts that are exact replicas of the whole (Peitgen et al., 1991). Thus, four exact copies of the Koch curve can be obtained by scaling it up by a factor of three along its base line, making its fractal dimension $D = \log 4 / \log 3 \approx 1.26$.

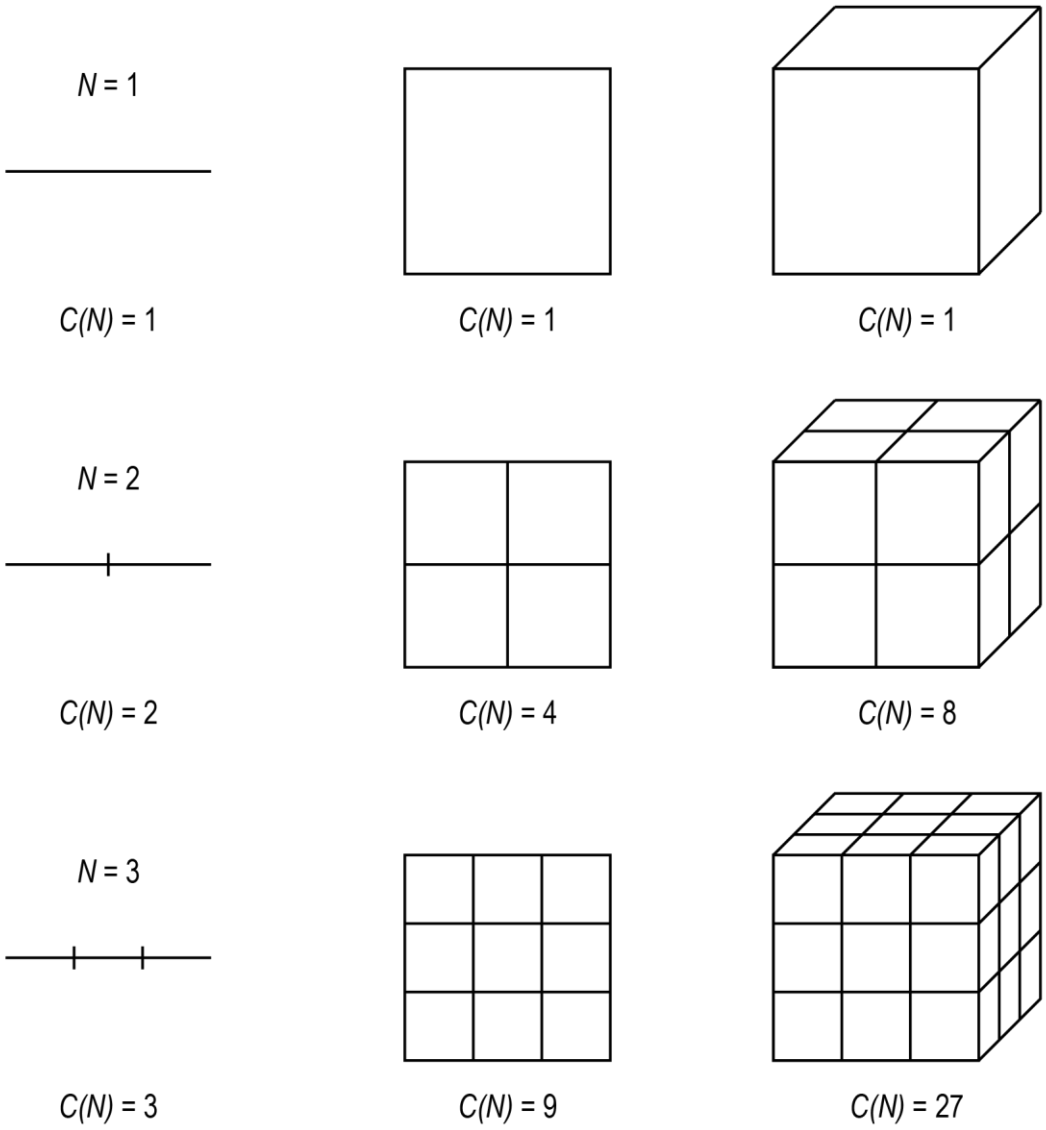

Figure 2.6. Relationship between the dimension and scaling of an object. A *D*-dimensional object scaled up by a factor of *N* can be partitioned into N^D copies of itself. Adapted from Pilgrim and Taylor (2018).

Except for some well-defined mathematical fractals such as the Koch curve, determining fractal dimension, specifically for natural shapes, is not straightforward. Therefore, many methods have been developed for estimating the fractal dimension of the structures that are not exactly self-similar, but rather "statistically" self-

similar. Among them, box-counting is a frequently used technique for estimating the fractal dimension of real-world structures.

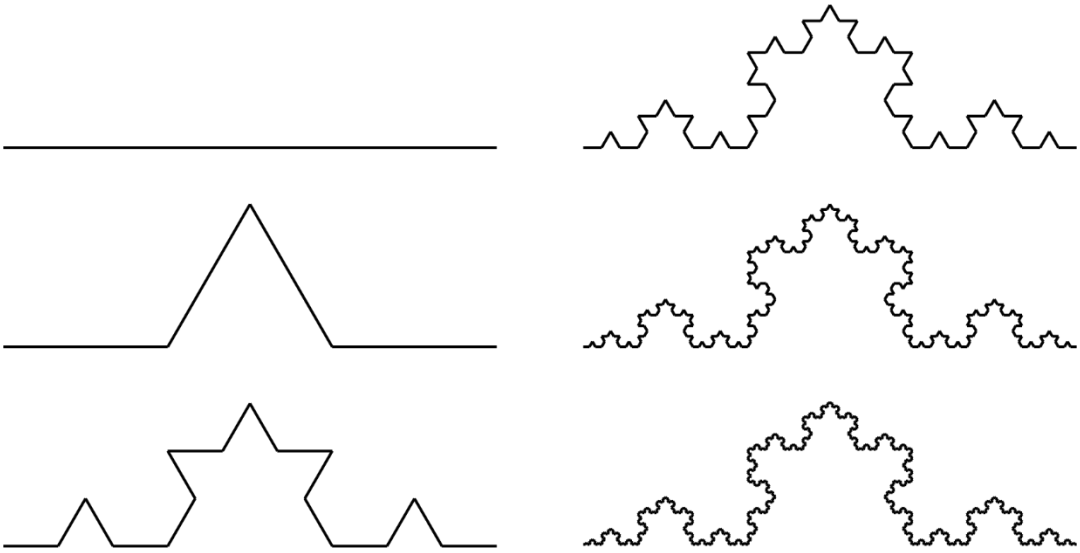

Figure 2.7. Construction steps of the Koch curve.

Box-counting method measures the scaling of the details of a fractal structure at varying resolutions as follows: the structure is superimposed on a square grid of size l and the number of boxes $N(l)$ covering the structure is counted. This process is repeated by varying the box size l (Fig. 2.8). In a self-similar structure, $N(l)$ changes in proportion to l^{-D}, where D is the box-counting dimension. Hence, D can be obtained by finding the slope of a $log(N(l))$ vs. $log(1/l)$ plot. Although the box-counting method was described here for the fractal structures that are embedded in two dimensions, it is straightforward to generalize the technique to other dimensions as well.

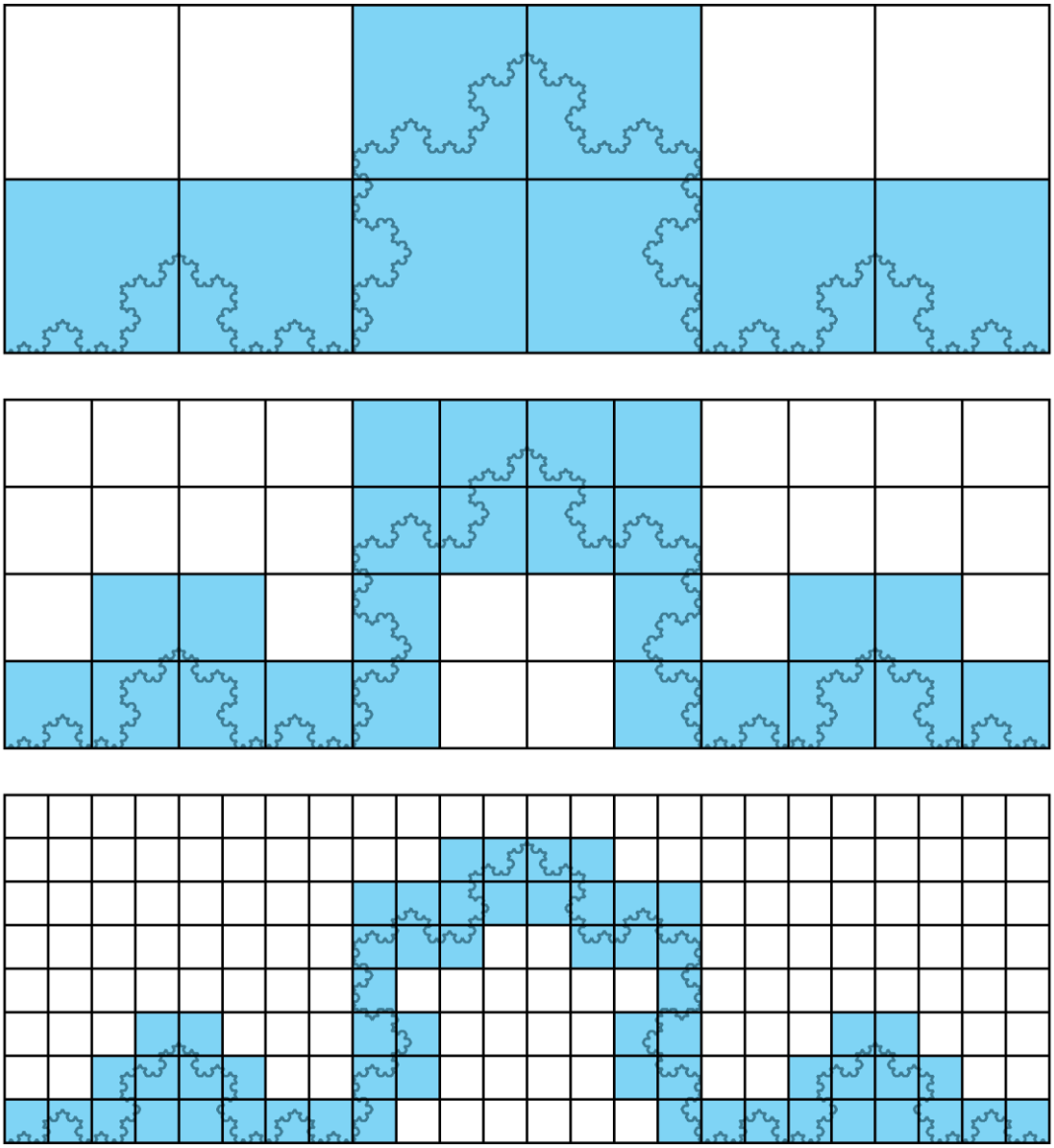

Figure 2.8. Estimating fractal dimension by the box-counting method. The number of boxes containing the structure at different scales, represent the amount of detail at those scales. Adapted from Pilgrim and Taylor (2018).

2.7 Fractal Analysis of Time-Series

Fractal property is not limited only to spatial objects. An important class of structures that can benefit from fractal analysis are time-series. A time-series is a variable quantity that fluctuates in time (e.g., stock market prices, atmospheric pressure and biosignals), and while lacking a spatial form, it can also exhibit fractal behavior. However, the methods developed for estimating the fractal dimension of spatial structures, including the box-counting method, are not applicable to time-series (Pilgrim & Taylor, 2018). This arises from the fact that the spatial shape of a time-series is inherently undefined, since it is embedded within two dimensions with different units, which allows arbitrary scales for the axes in a time-series plot. The fundamentally undefined geometric aspect ratio thus leads to inconsistent estimates of fractal dimension when using methods like box-counting (Fig. 2.9). This issue is mentioned again in Section 3.3.2 in the case of Katz fractal dimension.

The aforementioned ambiguity in estimating the fractal dimension of a time-series by conventional methods necessitates development of fractal analysis techniques that are insensitive to such artificial geometric parameters. In the following, three proposed techniques surveyed by Pilgrim and Taylor (2018) are briefly mentioned without going into the mathematical details.

The first approach views a time-series not as a geometric figure (without a well-defined aspect ratio), but an ordered record of a process with a quantifiable degree of randomness. The "Hurst exponent" H (Hurst, 1951) quantifies the randomness characteristic of a time-series via an autocorrelation measurement. Specifically, a Hurst exponent of 0.5 describes a purely random process, and for $0.5 < H < 1$, it represents a process exhibiting a positive autocorrelation, while in the range $0 < H < 0.5$, it represents a process exhibiting a negative autocorrelation (Fig. 2.10).

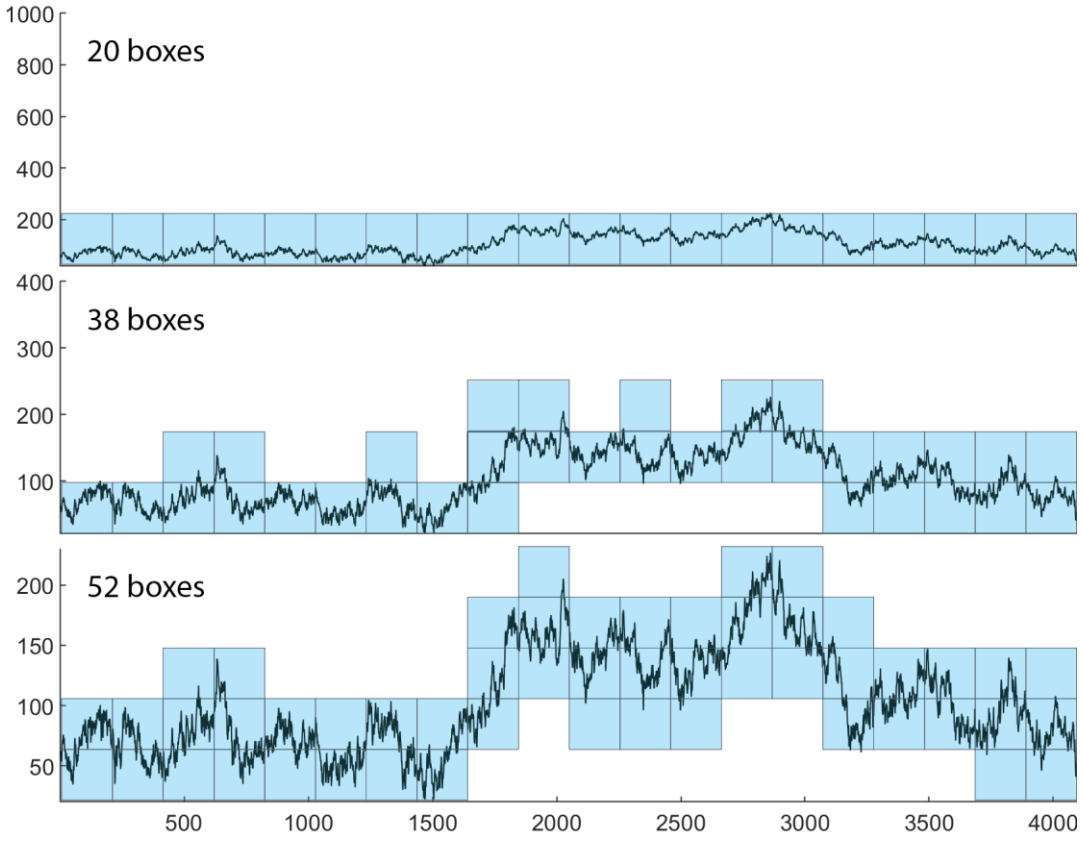

Figure 2.9. Same time-series at three different scales for the y-axis, while the scale of the x-axis remained unchanged. The box-counting method produces different results for different aspect ratios of a time-series plot.

The second method is called the "variation method" (Dubuc et al., 1989), and is conceptually similar to box-counting. The difference is that instead of drawing boxes, the structure is only varied in resolution along the time-axis, and the scale of the amplitude in each resolution is measured. A *log vs. log* plot similar to the one in the box-counting method is constructed, with the slope representing the fractal dimension.

"Adaptive fractal analysis" (Riley et al., 2012) is the third method, and is performed by modeling a time-series by means of best-fit lines at different resolutions. The root mean square error (RMSE) between the model and time-series varies in proportion

to w^H, where w is the resolution and H is the Hurst exponent. Thus, the slope of a *log(RMSE) vs. log(w)* plot yields the estimation of the Hurst exponent of the time-series.

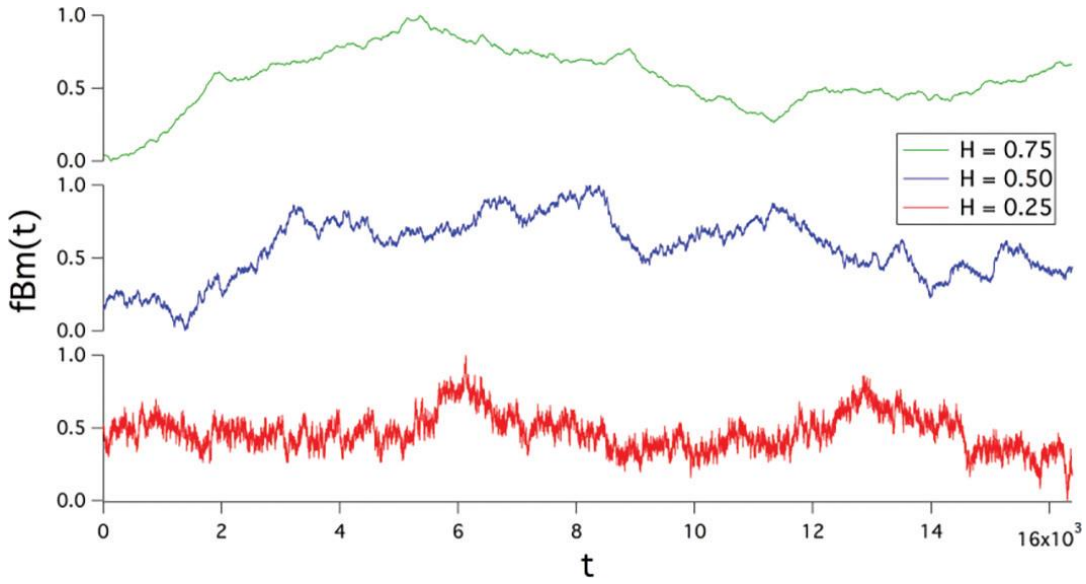

Figure 2.10. Fractal Brownian motion (fBm) time-series characterized by different Hurt exponents. From Pilgrim and Taylor (2018).

2.8 EEG As a *1/f* Process

Brain's rhythmic activity has been extensively studied in the literature, and brain oscillations in different frequency bands are linked to different psychophysiological states and cognitive functions (Campisi & La Rocca, 2014). In addition to the rhythmic activity, brain also exhibits arrhythmic fractal behavior in the form of a *1/f*-like trend in its power spectrum, i.e., power tends to decrease with the increase in frequency following a power-law function: $P \alpha 1/f^{\beta}$, where P is power, f is frequency and β is the "power-law exponent" (He, 2014). In general, the power-law exponent

($1 < \beta < 3$), Hurst exponent ($0 < H < 1$) and fractal dimension ($1 < D < 2$) of a time-series are related to one another by the following equations (Hinkel & Outcalt, 1995):

$$\beta = 2H + 1 \tag{2.1}$$

$$\beta = 5 - 2D \tag{2.2}$$

$$H = 2 - D\,. \tag{2.3}$$

According to He (2014), for decades, the *1/f*-like activity of the brain has been deemed an unimportant pink noise, hence it was often removed from the analyses to emphasize the brain oscillations. However, increasing evidence suggests that this scale-free component has an active role in brain's functioning, and can change in different mental states and generally over the course of time. Computational modeling studies have suggested some generative mechanisms for the scale-free brain activity, including irregular Poisson firing of cortical pyramidal neurons, which are reviewed in detail by He (2014).

2.9 Biometric Features Based on Signal Complexity

The arrhythmic *1/f* background of EEG power spectrum has also been investigated for subject-specific identity-bearing information. Demuru and Fraschini (2020) used the exponent and offset features obtained from a parametric modeling of the *1/f* trend of power spectrum (see Section 3.3.4.2) for subject identification. The recognition accuracy was 97.3 % among 95 subjects in the EO condition and 87.6 % among 100 subjects in the EC condition. The results of the study indicated that the aperiodic component of power spectrum was as distinctive for each subject as the periodic component.

The power-law exponent, Hurst exponent and fractal dimension are all measures that quantify signal complexity. Such measures have been less commonly employed in EEG-based biometrics, particularly in comparison to the features based on brain

oscillations, i.e., spectral band activities. In the following, three of the studies that employed complexity-based features are reviewed.

Mukai and Nakanishi (2020) employed fractal dimension by Higuchi's method (Higuchi, 1988) in the authentication of ultrasound evoked EEG signals from 10 subjects recorded by 14 electrodes. Fractal dimension features were classified using Euclidean distance and fused at the decision level, yielding an EER of 28.7 %.

Another measure of complexity is entropy, which quantifies the degree of disorder in a system. There are several types of entropy measures. As mentioned earlier in Section 2.5, Thomas and Vinod (2016) used sample entropy to identify from 109 subjects in the resting state conditions. Using a Mahalanobis classifier, maximum CRRs of 98.31 % and 96.94 % were obtained for beta band in the EO and EC conditions, respectively.

Mu et al. (2016) used fuzzy entropy to authenticate EEG signals recorded by two electrodes in the frontal region from 10 subjects. The visual stimuli of self-photos and non-self-photos were used for the elicitation of the EEG signals. Using a back propagation neural network, an average classification accuracy of 87.3 %, false acceptance rate of 5.5 % and false rejection rate of 5.6 % were obtained.

In addition to the mentioned studies, Alzahab et al. (2021) and Moctezuma and Molinas (2019) employed complexity-based features in fusion with other features for subject authentication.

CHAPTER 3

METHODS AND MATERIALS

In this chapter, our methodology is presented. All feature extraction routines were performed using MATLAB (R2019b, The Mathworks, Inc., Natick, MA) on an Intel(R) Xeon(R) CPU E5- 2650 0 @ 2.00GHz 2.00 GHz processor. Classification models were implemented in a separate computer using the Scikit-learn library (https://www.scikit-learn.org) in Python 3. Codes for feature extraction and classification are available at https://github.com/RezaYahyaei/Paper2022.

3.1 Dataset

This study benefited from the publically available PhysioNet EEG Motor Movement/Imagery Dataset (Goldberger et al., 2000), a frequently utilized database in EEG biometric studies (Das et al., 2019; DelPozo-Banos et al., 2015; Demuru & Fraschini, 2020; Fraschini et al., 2014, 2018; Jijomon & Vinod, 2018; Keshishzadeh et al., 2016; La Rocca et al., 2014; Lai et al., 2019; Ma et al., 2015; Monsy & Vinod, 2020; Schons et al., 2017; Singh et al., 2015; Sun et al., 2019; Thomas & Vinod, 2016, 2018; Wang et al., 2019a, 2019b, 2020; Yang et al., 2018). It comprises EEG recordings from 109 participants in 14 experimental runs, including two baseline runs of resting state conditions with eyes-open (EO) and eyes-closed (EC), both lasting one minute. Data were recorded using a BCI2000 system (http://www.bci2000.org) with 64 electrodes and a sampling rate of 160 Hz. Electrodes were arranged according to the international 10-10 system (Fig. 3.1). All EEG signals were referenced to the average of the signals coming from earlobes.

As EEG is known to be sensitive to human mental states (see Section 2.3), spontaneous brain data acquired during resting state have been mostly preferred for biometric recognition to keep the intra-individual variations in brain activity as low as possible. Thus in the current study, the EO and EC resting state data were used for the evaluation of the proposed methodology.

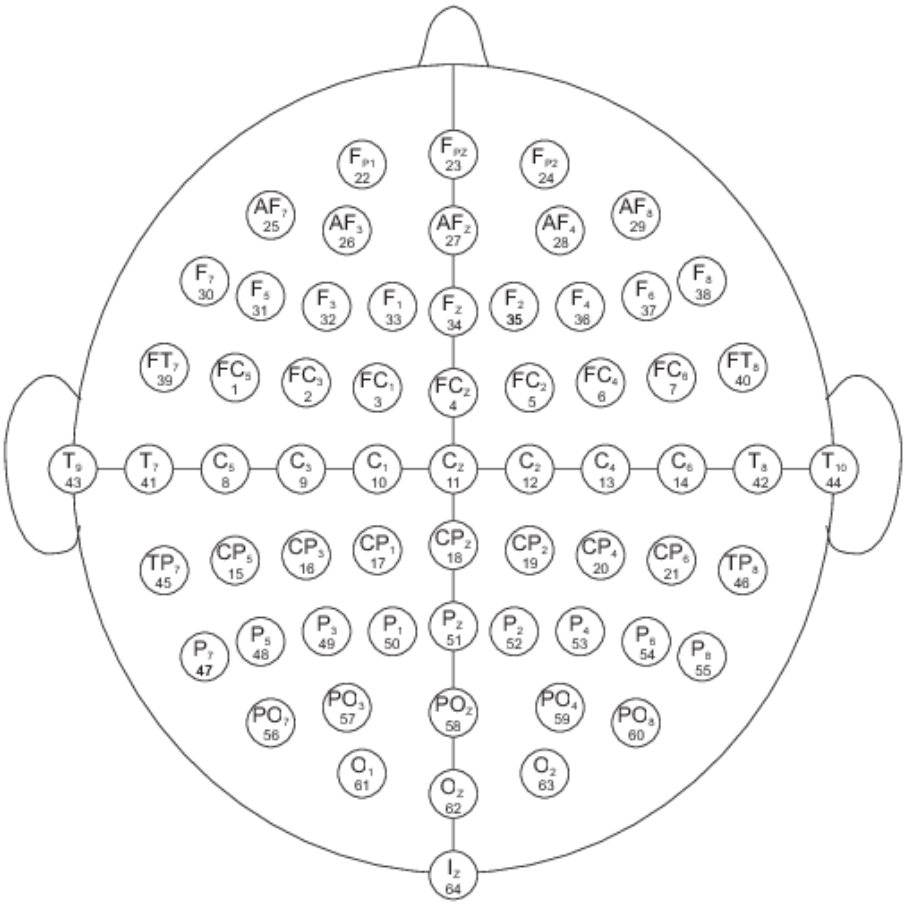

Figure 3.1. Electrode arrangement for the PhysioNet dataset. From PhysioNet (2009).

3.2 Preprocessing

For each subject and condition, the recorded signals were split into six non-overlapping segments of 10 seconds to generate samples, five of them for training the model and one for testing it (Fig. 3.2). A low-pass FIR filter with a cut-off frequency of 50 Hz was applied to each segment separately to eliminate the noise-ridden higher frequency components, including the 60 Hz power line frequency and to retain only the targeted range of brain's rhythmic activity – i.e., the five canonical frequency bands (see Section 2.4).

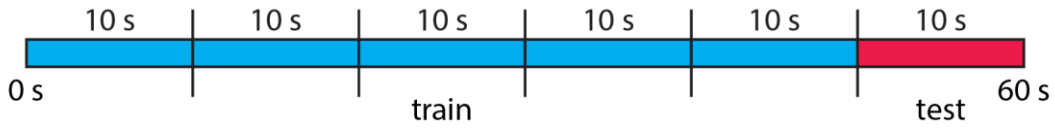

Figure 3.2. Segmentation of the EEG recordings. The arrangement of the segments does not imply their chronological order.

3.3 Feature Extraction

Despite the existence of studies where EEG signals themselves were used as inputs to a biometric system, most of the time, other high-level representative information, called features, are extracted from the signals and then fed into a biometric classification model. Features can be categorized based on the specific aspect of the signal that they are describing (Table 3.1).

In this thesis, a new feature, called the mean curve length (MCL; Section 3.3.1), is proposed as a potential EEG-based biometric for person identification and authentication. It is derived from the Katz fractal dimension (Section 3.3.3), hence goes under the category of signal-complexity-based features.

Table 3.1 Some of the features used in EEG-based biometrics divided into different categories.

Category	Features
Time domain	• Raw/preprocessed signal • Event-related potential • Autoregressive coefficients
Frequency domain	• Power spectral density • Frequency band specific power • Wavelet transform
Statistics	• Mean • Variance • Skewness • Kurtosis
Complexity	• Hurst exponent • Power-law exponent • Lempel-Ziv complexity Entropy: • Fuzzy entropy • Approximate entropy • Sample entropy Fractal dimension: • Petrosian fractal dimension • Katz fractal dimension • Higuchi fractal dimension

Table 3.1 (continued)

Category	Features
Functional connectivity	Power-based: • Pearson's correlation Phase-based: • Phase-locking value • Spectral coherence • Phase-lag index Information-based: • Mutual information Causal: • Granger causality
Network	• Weighted nodal degree • Eigenvector centrality • Pagerank centrality

3.3.1 Mean Curve Length (MCL)

Curve length (CL) was originally proposed by Esteller et al. (2001) as a computationally efficient substitute for the Katz fractal dimension (Section 3.3.2). As the name suggests, curve length is the sum of the linear distances between successive points on a curve. For the case of EEG, the so-called curve is basically equivalent to the signal trace. Since the time-axis contributes equally to the distances for a fixed sampling rate, it is not taken into account while computing CL. Hence, CL is the sum of the absolute value of the first-order finite difference (discrete derivative) for a time-series. Mean curve length (MCL) is simply obtained by averaging CL:

$$MCL = \frac{1}{N-1}\sum_{n=0}^{N-2}|\Delta_1 x(n)| = \frac{1}{N-1}\sum_{n=0}^{N-2}|x(n+1) - x(n)| \tag{3.1}$$

where *N* is the signal length. Fig. 3.3 exhibits a visual illustration of MCL.

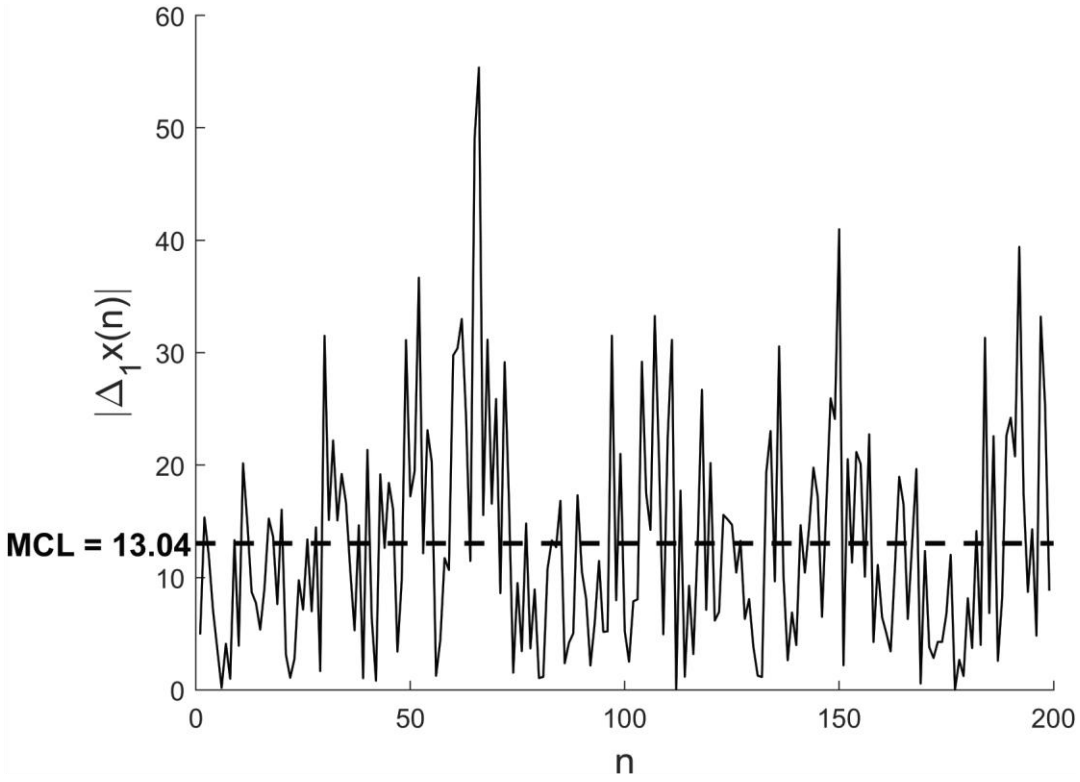

Figure 3.3. An exemplary illustration of the mean curve length that can be considered as the mean of absolute value of first-order finite difference (discrete derivative) of a signal.

In the generalized form of CL, the so-called short-time average magnitude difference function (AMDF), the difference can be computed with a selected time delay – *x*(*n*

+ τ) - $x(n)$, where τ is an integer. This enables AMDF to detect changes in an extended number of frequencies; hence for this capability, it has generally been applied in speech signal processing for time-delay estimation (Chen et al., 2005) and pitch detection (Hui et al., 2006). Özkurt et al. (2006) used it for seizure detection, and compared its performance with conventional CL. A short-time AMDF was introduced by Akgül et al. (2000) in order to capture sleep spindle related regularities from sleep EEG signals. A more generalized form of AMDF was defined by adding an integer-wise degree in order to identify nonlinear properties with an application to Parkinson's disease subcortical and cortical signals (Özkurt et al., 2020). Moreover in the same study, those generalized AMDF values were shown to be correlated with clinical motor symptoms.

3.3.2 Katz Fractal Dimension (KFD)

Katz (1988) introduced a formulation for the fractal characterization of waveforms, which are two-dimensional curves that monotonically move forwards in one dimension (e.g., the time dimension). This can be especially useful for analyzing and comparing complex waveforms such as EEG signals. The fractal dimension D as defined by Katz (1988) is given by

$$D = \log(L) \,/\, \log(d)\,, \tag{3.2}$$

where L is the curve length in two dimensions and is defined as

$$L = \sum_{n=0}^{N-2} \sqrt{(x(n+1) - x(n))^2 + \Delta t^2}\,, \tag{3.3}$$

where Δt is the constant unit of time (i.e., the sampling period) and d is the curve diameter (or planar extent), defined as the farthest distance between the starting point and any other point on the curve:

$$d = \max \sqrt{(x(n) - x(1))^2 + (t(n) - t(1))^2} \tag{3.4}$$

for $n = 0, 1, \ldots, N\text{-}1$. Notice that unlike MCL, the time-axis has to be taken into account for computing the Katz fractal dimension (KFD), since it does not equally contribute to the distances in Eq. 3.4.

The ratio in Eq. 3.2 compares the actual length of the curve with the minimum length required to create a curve of the same spatial extent. Complex and convoluted curves tend to have higher fractal dimensions, since they can fit a long length within a small extension of space, i.e., they fill more of the space (Fig. 3.4).

Figure 3.4. Two curves with different degrees of convolution and their flattened real sizes. Curve 2 has a greater fractal dimension than curve 1, since it fits a longer length within the same spatial extent.

Since arbitrary units of length for the definition in Eq. 3.2 produce different results, a standard unit, denoted as a, describing the average distance between the successive points was defined in order to normalize KFD (Katz, 1988):

$$D = \frac{\log(L/a)}{\log(d/a)} = \frac{\log(m)}{\log(m) + \log(d/L)} \tag{3.5}$$

where $m = L/a$ is the number of steps on the curve. Despite this normalization, the difference between the units of *x*- and *y-axis* is not taken into account for a typical time-series (see Section 2.7). This is important, because by considering a time-series as a geometrical object, different values of fractal dimension can still be generated by choosing arbitrary scales for the time and amplitude axes.

The unit of time Δt has been treated differently in various implementations of KFD. For instance, in one implementation (Monge-Álvarez, 2021), Δt was taken as one, while in another (Vallat & Van Der Donckt, 2021), the time dimension was altogether ignored. Depending on the value of Δt, one can obtain different values for the fractal dimension of a given curve (see Appendix A). It is helpful to understand the effect of this parameter by considering the extreme cases. When the unit of time goes towards the infinity, the relative size of signal amplitude becomes so negligible that any curve stretches into a virtually straight line with a fractal dimension of approximately one. In the other extreme when the unit of time is zero (i.e., KFD is computed in one dimension), the curve diameter would merely be the largest peak in a signal. This would lead to inconsistent results because of the inevitable variations in signal amplitude, particularly caused by noise, and the elimination of the normalization for signal length. In our own implementation, Δt was set to one to have a close but smaller magnitude than the average distance along the amplitude-axis (Eq. 3.3) so that the effect of the latter remains dominant. On the other hand, one can also consider the unit of time as a hyperparameter for tuning during the classification stage.

3.3.3 Derivation of MCL from KFD

In the previous section it was mentioned that Katz's formulation of fractal dimension has an ambiguity with regard to time-series such as EEG signals, since the distances

along the two dimensions have different units. In addition to that, some combinations of values for the parameters in Katz's formulation (i.e., *m*, *L* and *d* in Eq. 3.5) lead to inconsistent results (Esteller et al., 2001). To overcome these problems, Esteller et al. (2001) proposed that the logarithms in Katz's formulation could be dropped to obtain a more computationally efficient feature without compromising the detection capability. After eliminating the logarithmic functions in the numerator and denominator, Eq. 3.2 becomes *L/d*. Here, *d* can be considered as a normalization factor, which does not change significantly among time segments of equal length (Esteller et al., 2001), and hence can be taken as a constant. With *d* being a constant, *L* is no longer needed to be calculated in two dimensions (see Section 3.3.2), thus it would be equivalent to CL (Section 3.3.1). Finally, substituting the number of steps *n* for the curve diameter *d* leads to the definition of MCL in Eq. 3.1. MCL is a well-defined measure computed in one dimension, avoiding the problems of possibly singular or improper outputs (Esteller et al., 2001) and dimensional unit inconsistency existent in KFD. Moreover, MCL has a strong correlation with KFD (Pearson's $r = 0.96$, $p < 10^{-15}$ in the employed dataset; see Appendix B).

3.3.4 Other Features

We included several of the highly discriminative features commonly used in EEG-based biometrics in order to compare with MCL on the same dataset. Some of the employed features are as follows: power spectral density (PSD) (Thomas & Vinod, 2018), aperiodic component (AP) of PSD (Demuru & Fraschini, 2020) and autoregressive (AR) coefficients (Keshishzadeh et al., 2016). In addition, we included two common cross-channel metrics of functional connectivity that quantify phase synchronization: phase-locking value (PLV) (Wang et al., 2019a) and spectral coherence (COH) (La Rocca et al., 2014). It has been shown that pairwise connectivity measures between channels may yield a better biometric recognition than single-channel spectral measures (La Rocca et al., 2014).

3.3.4.1 Power Spectral Density (PSD)

One way of extracting the PSD of a signal is to transform it from time-domain to frequency-domain power representation. With this approach, all of the spectral content of the signal is obtained in the form of a spectral power distribution over an array of frequency bins. The width of the frequency bins, which represents the frequency resolution, depends on the sampling frequency of the signal. The transformation, generally known as the power spectral estimation, can be carried out using a vast variety of techniques; they are generally divided into i) classical non-parametric methods (e.g., periodogram and multitaper), which are mostly based on the Fourier analysis, and ii) parametric methods (e.g., autoregressive and moving average), which involve estimating the parameters of a time-series model.

The second way of PSD feature extraction is to band-pass filter a signal in a select number of frequency bands and compute their powers. This does not produce all spectral information of the signal, but it provides more control over the frequency ranges from which one wants to extract the PSD features. The conventional way of selecting frequency bands is from the canonical bands (i.e., delta, theta, alpha, beta and gamma). Filtering can also be done via various types of discrete-time filters. Discrete-time filters are commonly categorized as FIR and IIR (finite and infinite impulse response) filters. For most situations, FIR filters are preferred over IIR filters, because although FIR filters have slightly more computational cost, they are "more stable and less likely to introduce nonlinear phase distortions" (Cohen, 2014).

In our case, the second approach of using an FIR filter was followed. In accordance to the frequency band results in the previous EEG-based biometrics literature (see Section 2.5), we computed the signal power (i.e., the time average of the signal amplitude squared) within the frequency bands of beta (12–30 Hz) and gamma (30–45 Hz) and concatenated them into a single feature vector.

3.3.4.2 Aperiodic (AP) Component of PSD

In the power spectrum of an EEG signal, the power decreases as a function of an increase in the frequency following a *1/f* shape (Cohen, 2014; see Section 2.8). The *1/f* background is the aperiodic component of the PSD on which the periodic content of the signal is added (Fig. 3.5). Thus, the power value corresponding to a frequency bin is the sum of its aperiodic component and the spectral power of that frequency. The aperiodic component *L* is modeled as

$$L(f) = b - \log_{10}(k + f^{x}) , \tag{3.6}$$

where f is the "array of frequency values", *b* is the "broadband offset", *k* is the "knee" and *x* is the "exponent of the aperiodic fit" (Donoghue et al., 2020). When this equation is fitted to the PSD of a signal, three parameters, namely *b*, *k* and *x* are obtained.

We used the *Fitting Oscillations and One Over F* (FOOOF) toolbox (Donoghue et al., 2020), which is specifically developed for the analysis of periodic and aperiodic properties of electrophysiological data, to fit the aperiodic component of the EEG signals. The knee parameter, which "defines a bend in the aperiodic *1/f* like component", is optional and defaults to zero when not specified (Donoghue et al., 2020). Since it is less important than the other two parameters, we did not use it. The offset (*b*) and exponent (*x*) parameters were obtained using the *fooof* function in the toolbox. The primary input to this function is the PSD of a signal. The PSD was obtained by Matlab's *pwelch* function, which uses Welch's averaged periodogram method to estimate the power spectrum. For the *pwelch* parameters, considering that each data segment is 10 seconds, a Hann window of 2 seconds with 50 % overlap was deemed appropriate. The frequency range for curve fitting was set to 1 – 40 Hz.

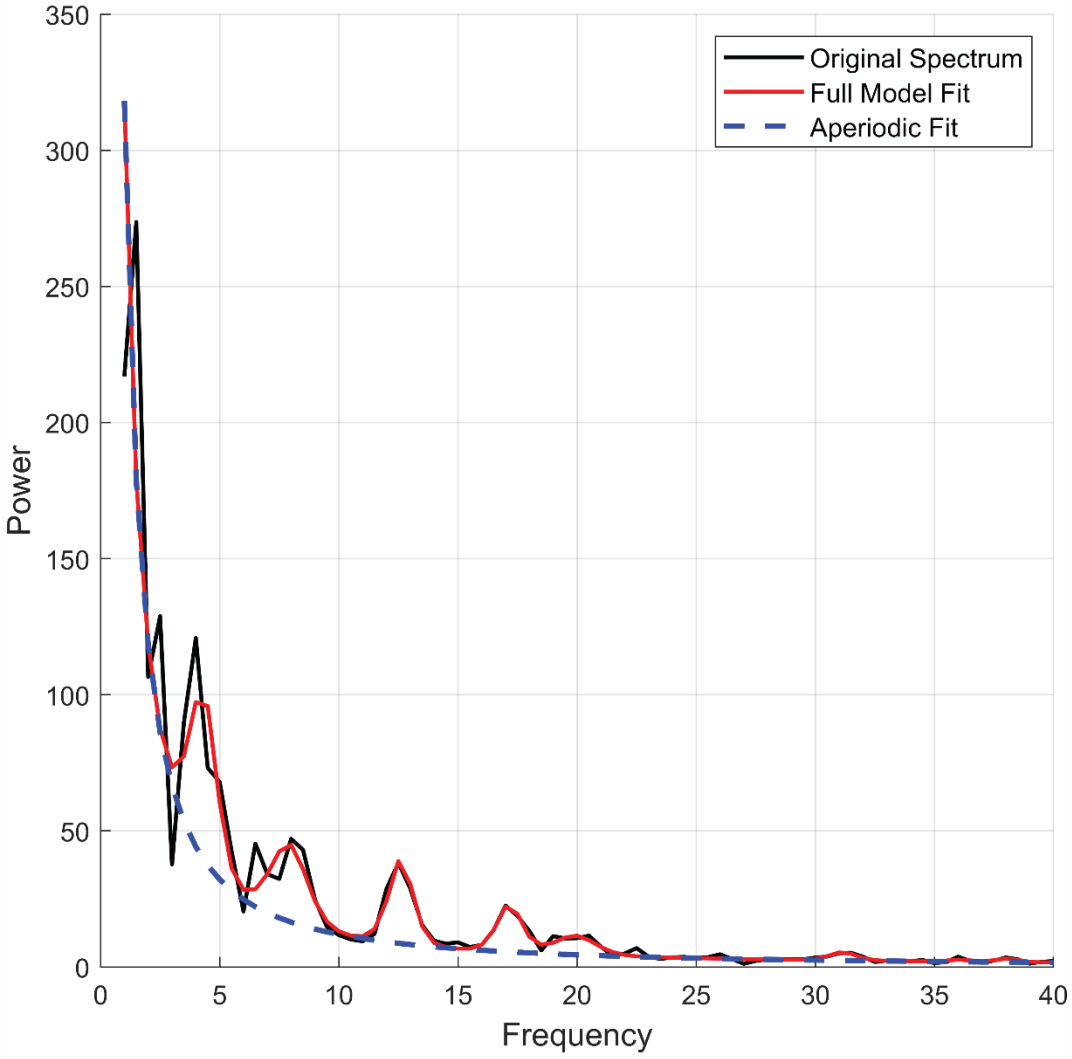

Figure 3.5. Modeling of the *1/f* aperiodic component of the power spectrum of an EEG signal.

3.3.4.3 Phase-Locking Value (PLV)

Phase locking value (PLV; Lachaux et al., 1999) is a phase-synchrony-based functional connectivity measure. It is calculated as the time average of the phase difference between two electrodes:

$$PLV = \frac{1}{N}\left|\sum_{n=1}^{N} e^{i(\varphi_{x(n)}-\varphi_{y(n)})}\right| \tag{3.7}$$

where N is the length of the time segment, and $\varphi_{x(t)}$ and $\varphi_{y(t)}$ are the phase time-series of the two electrodes. PLV values range from zero to one, with zero meaning no synchrony and one indicating perfect synchronization.

Phase time-series can be obtained from the analytic signal representation, which is a complex time-series. A more intuitive way to represent a complex time-series is by using Euler's formula $me^{i\varphi}$, which describes a complex number as a vector on the complex plane, with length m and angle φ relative to the positive real-axis. For a complex number $a + ib$,

$$m = \sqrt{a^2 + b^2} \tag{3.8}$$

$$\varphi = \sin^{-1} b/a\,. \tag{3.9}$$

One method of obtaining the analytic signal is by applying the Hilbert transform to the original signal. Here, the original signals were the band-pass filtered EEG signals. Based on the findings in the previous EEG-based biometrics literature (see Section 2.5), beta (12–30 Hz) and gamma (30–45 Hz) bands were selected for PLV feature extraction. For each frequency band, PLV was computed between all pairs of electrodes. Having 64 electrodes, the size of the PLV feature vector for each band became 64 × 63 / 2 = 2016. Lastly, the feature vectors corresponding to the two frequency bands were concatenated.

3.3.4.4 Spectral Coherence (COH)

Spectral coherence (COH) is another phase-synchrony-based functional connectivity measure. In comparison to PLV, COH also includes the signal amplitude in addition to its phase:

$$COH = \frac{\left|\frac{1}{N}\sum_{n=1}^{N} m_{x(n)} m_{y(n)} e^{i(\varphi_{x(n)} - \varphi_{y(n)})}\right|^2}{\left(\frac{1}{N}\sum_{n=1}^{N} m_{x(n)}^2\right)\left(\frac{1}{N}\sum_{n=1}^{N} m_{y(n)}^2\right)} \tag{3.10}$$

where N is the length of the time segment, $m_{x(t)}$ and $m_{y(t)}$ are the amplitude time-series, and $\varphi_{x(t)}$ and $\varphi_{y(t)}$ are the phase time-series of the two electrodes (Cohen, 2014). COH values also range from zero to one, with zero meaning complete independence, and one meaning complete coherence.

The definition of COH is similar to the definition for correlation; COH can be viewed as the correlation between two analytic signals. By adopting the dot product notation (.) between two vectors, Pearson's correlation is computed as

$$r = \frac{x.y}{(x.x)(y.y)}, \tag{3.11}$$

where x and y are mean-subtracted time-series vectors. Since analytic time-series are complex numbers, a conjugate transpose (which negates the phase time-series) is applied to the right-hand side vector in the inner product. Thus, the correlation of two complex time-series yields an almost identical result (by excluding the extra power of two in the numerator) to Eq. 3.10. In the context of time-series spectral analysis, ($x.y$) is the cross-spectrum, and ($x.x$) and ($y.y$) are the auto-spectra of the time-series.

The analytic signals were obtained by applying the Hilbert transform on the band-pass filtered EEG signals. Based on the findings in the previous EEG-based biometrics literature (see Section 2.5), beta (12–30 Hz) and gamma (30–45 Hz) bands were selected for COH feature extraction. For each frequency band, COH was computed between each pair among 64 electrodes, which amounted to 64 × 63 / 2 = 2016 features. The features corresponding to the two frequency bands were concatenated to construct a single feature vector.

3.3.4.5 Autoregressive (AR) Coefficients

EEG signals can be modeled as stochastic processes where each value in the time-series is predicted as a linear combination of the past values added by a stochastic term:

$$x(n) = -\sum_{k=1}^{p} a(k)x(n-k) + \varepsilon(n) \tag{3.12}$$

where x is the time-series, p is the model order, a_k are the model coefficients, and ε is an independent stochastic variable with zero mean (Bos et al., 2002). Among the possible AR coefficient estimation techniques, Burg's method has been mostly preferred in the literature for its lower computational complexity and better performance (Gui et al., 2019; La Rocca et al., 2013). Here, Matlab's *arburg* function was employed to estimate the AR coefficients using Burg's method. A model order of five was selected based on an EEG biometrics study (Keshishzadeh et al., 2016) which used the same dataset as here.

3.4 Classification

Classification is a supervised machine learning approach where a classifier model is constructed and trained to identify to which class an observation belongs. In the context of biometrics, the observation is an unknown person and the class is their identity. Features that are extracted from individual EEGs, along with their class labels, comprise the training data. Usually the features for every person are a set of numeric values that form what is called a feature vector. Each feature vector is labeled with its corresponding class label (which is also encoded in an integer value) – hence the name supervised learning. From these examples, the classifier learns to map the feature vectors to the correct labels, thus when presented with an unknown feature vector, the classifier can identify to which class it belongs. Generally, a fraction of the training data is reserved for testing the model performance.

Classification methods employed in EEG biometric studies divide into two main paradigms: i) conventional classifiers, in particular those that are distance-based or similarity-based, and ii) deep learning neural networks, where convolutional neural networks (CNN) are often used (Table 3.2). Each of the classifiers has its own advantages and disadvantages, therefore there is no best classifier for all sorts of features and conditions.

In this study, we employed a Mahalanobis classifier (Section 3.4.1) both for subject identification and authentication tasks. A modification of this classifier (Section 3.4.2) was also proposed for high-dimensional features, i.e., those having feature vectors with a large number of elements.

3.4.1 Mahalanobis Distance

We preferred a Mahalanobis distance-based classifier in our study for the following reasons:

- low computational cost

- producing closed-form solutions
- no requirement for parameter tuning or optimization iterations
- providing scores (distances) that enable applicability for authentication

Moreover, Mahalanobis distance is scale-invariant, works for both Gaussian and non-Gaussian data and has shown to yield the best performance in K nearest neighbor classifiers (KNN) among the other distance metrics – namely, Kullback-Leibler, Euclidean, Manhattan, Hamming and Minkowski distances (Walters-Williams & Li, 2010). Mahalanobis classifier has already been applied in EEG-based biometrics (La Rocca et al., 2014; Thomas & Vinod, 2016; Wang et al., 2020) and has produced comparable results to the other more sophisticated classifiers.

Table 3.2 Some common classifiers used in EEG-based biometrics.

Classifier Type	**Classifiers**
Conventional	Similarity-based: • Correlation • Cosine similarity Distance-based: • Euclidean distance • Mahalanobis distance • Manhattan distance Others: • Support vector machine (SVM) • Random forest • Linear discriminant analysis (LDA)
Deep learning	• Multi-layer perceptron (MLP) • Convolutional neural network (CNN) • Recurrent neural network (RNN)

Computing Mahalanobis distance requires the estimation of the inverse covariance matrix for each class (subject) distribution. Since the number of samples for each class is small (five samples), the individual covariance matrices cannot be robustly estimated. To address this, we followed a common procedure consisting in approximating the covariance matrix of each class to be equal to the covariance matrix computed from all classes (La Rocca et al., 2014). This way, only one covariance matrix was stored in the database. Following this approach, for the n features of each feature set, an $(n \times n)$ covariance matrix was computed using 5×109 samples (for 5 segments and 109 subjects). After acquiring the inverse covariance matrix Σ^{-1}, the square Mahalanobis distance $d_{u,n}^2$ between an unidentified observation's feature vector η_u and a class centroid μ_n was calculated according to the definition:

$$d_{u,n}^2 = (\eta_u - \mu_n)^T \Sigma^{-1} (\eta_u - \mu_n) \tag{3.13}$$

where $u, n \in \{1, 2, \ldots, C\}$, with C and superscript T denoting the number of classes and the matrix transpose, respectively. Class centroids are the subject templates that were stored in the database during user registration. They are the feature vectors that were obtained by averaging the five sample feature vectors (corresponding to the five segments designated for training, as described in Section 3.2) for each subject.

Classification (i.e., subject identification) using Mahalanobis distance is performed by assigning the identity of an unknown observation to the class distribution with the minimum distance:

$$\hat{n} = argmin_n d_{u,n}^2 \, . \tag{3.14}$$

For subject authentication, a distance threshold was admitted, such that the observations within that distance were accepted as belonging to the authorized person, while the ones farther than that were rejected as impostors. An appropriate threshold can be determined by taking into account the trade-off between false acceptance/rejection rates (see Section 3.5).

3.4.2 Modified Mahalanobis Distance

Mahalanobis classifier suffers from a deficiency with regard to high-dimensional features such as PLV and COH, as the covariance matrix can become extremely large, possibly leading to a memory crash in a common processor. Therefore, we modified the implementation of Mahalanobis distance in order to incorporate a dimensionality reduction. This was achieved by taking advantage of the fact that Mahalanobis distance is equivalent to Euclidean distance for a whitened distribution (Kessy et al., 2018), thus allowing it to be computed in two separate steps: whitening the data and calculating the Euclidean distance.

Whitening, or sphering, is a linear transformation of a vector of random variables (in this case, features) that involves: removing the correlations between the variables (decorrelation), setting the variances of all variables to one (standardizing) and optionally, setting the means of all variables to zero (centering) (Fig. 3.6). A whitened vector z with an identity covariance matrix is obtained by applying a whitening matrix W to a random vector x:

$$z = Wx\ . \tag{3.15}$$

Since z has an identity covariance matrix, it follows that

$$zz^T = Wxx^TW^T = W\Sigma W^T = I\ , \tag{3.16}$$

and thus

$$W(\Sigma W^T W) = W\,, \tag{3.17}$$

which is satisfied when

$$W^T W = \Sigma^{-1}\,, \tag{3.18}$$

or

$$W = \Sigma^{-1/2} \tag{3.19}$$

(Kessy et al., 2018). Thus, the Mahalanobis distance formula (Eq. 3.13) can be rewritten as

$$\begin{aligned} d_{u,n} &= \sqrt{(\eta_u - \mu_n)^T \Sigma^{-1} (\eta_u - \mu_n)} \\ &= \sqrt{(\eta_u - \mu_n)^T W^T W (\eta_u - \mu_n)} \\ &= \sqrt{z^T z}\,, \end{aligned} \tag{3.20}$$

which is the Euclidean distance between $W\eta_u$ and $W\mu_n$.

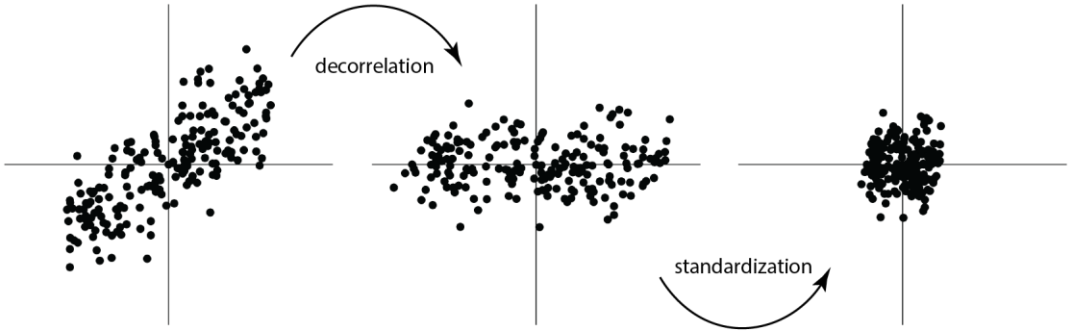

Figure 3.6. Whitening process illustrated on simulated samples with two correlated random variables.

By using principal component analysis (PCA), one can perform whitening as well as dimensionality reduction before calculating the Euclidean distance. Standard PCA only decorrelates data, where the variances of the transformed features indicate their importance. Dimensionality reduction is performed by eliminating the transformed features with the least variances. PCA with whitening furthermore standardizes the remaining transformed features (Fig. 3.7).

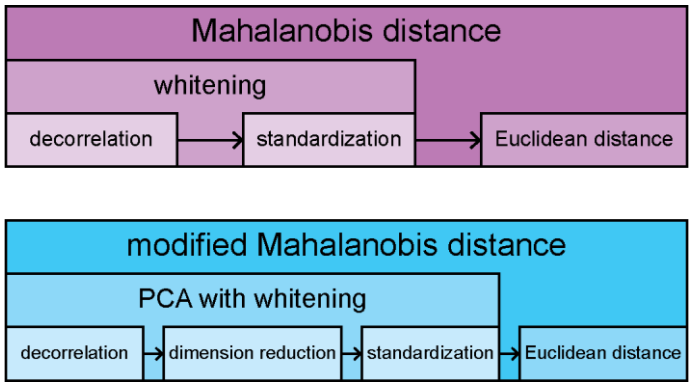

Figure 3.7. Mahalanobis distance and its modified implementation incorporating dimensionality reduction.

PCA not only decreases the computational complexity by reducing the size of feature vectors, but also significantly improves the classification performance by helping to avoid the curse of dimensionality. In this study, we used Scikit-learn's *PCA* class to perform PCA with whitening. The number of retained components (features) should be specified when constructing an instance of this class. Alternatively, this class also provides the functionality to automatically find the minimum number of components such that a user-specified fraction of the total variance is retained.

Using Scikit-learn's *PCA* and *NearestCentroid* classes, a two-step classification pipeline was constructed. Euclidean distance was set to be the metric for the *NearestCentroid* class instance. For low-dimensional features (MCL, KFD, PSD and AP) all of the feature elements were kept (i.e., whitening without dimensionality reduction). For high-dimensional features (PLV, COH and AR), a dimensionality reduction with a 99 % retained variance was included.

3.5 Evaluation

In order to evaluate the proposed feature and methodology and to make comparisons, we used the following standard metrics reported in the literature for the evaluation of EEG-based biometric systems (Gui et al., 2019).

Correct recognition rate (CRR) is used to assess the identification performance of a biometric system and is defined as

$$CRR = \frac{number\ of\ correct\ identifications}{number\ of\ all\ identifications}. \tag{3.21}$$

In this work, CRR values were computed in a leave-one-out cross-validation fashion as follows: from the six segments corresponding to each subject (see Section 3.2), one was leaved out for testing the model and the remaining five segments were used for its training. This was carried out for all six combinations of train/test set split.

Subsequently, the mean and standard deviation of the CRR values were computed over the six cross-validation iterations.

In contrast to the identification performance, authentication can be evaluated by a variety of means, which are mostly interrelated. The basic metrics consist of: true acceptance rate (TAR), true rejection rate (TRR), false acceptance rate (FAR) and false rejection rate (FRR), defined as follows:

$$TAR = \frac{TP}{TP + FN} \tag{3.22}$$

$$TRR = \frac{TN}{TN + FP} \tag{3.23}$$

$$FAR = \frac{FP}{FP + TN} \tag{3.24}$$

$$FRR = \frac{FN}{FN + TP} \tag{3.25}$$

where TP, TN, FP and FN denote the number of true positives, true negatives, false positives and false negatives, respectively. One problem with these metrics is that they change as a function of the threshold value. To obtain a unique value of evaluation, one can select two basic metrics with a trade-off relationship and plot their co-variation as a function of the threshold (Fig. 3.8). One type of such plot that is regularly used in the EEG-based biometrics literature is the plot of FRR versus FAR, known as the detection error trade-off (DET) curve. A unique metric of performance that can be extracted from these plots is the area under the curve (AUC). The second unique metric that is more often used is the equal error rate (EER); it is the common error rate at the threshold where FRR and FAR are equal (Fig. 3.8). Lower EER indicates better authentication performance.

Plotting a DET curve requires finding FRR and FAR values over a range of thresholds. We employed Scikit-learn's *roc_curve* function for this purpose. Given a set of pairwise distances, together with labels indicating whether they are intra-

class (genuine match) or inter-class (impostor match) distances, the function returns FAR and TAR values over a suitable range of thresholds generated by the function itself. Subsequently, FRR can simply be obtained by calculating 1-TAR (Eq. 3.22 and 3.25).

Within each cross-validation iteration, all pairwise distances between the test set and the templates (generated during the training) were stored. The test set and the template set both consisted of 109 elements corresponding to the subjects. Thus for the 6 cross-validation runs, there were 6 × 109 genuine and 6 × (109 × 108) impostor matches in total.

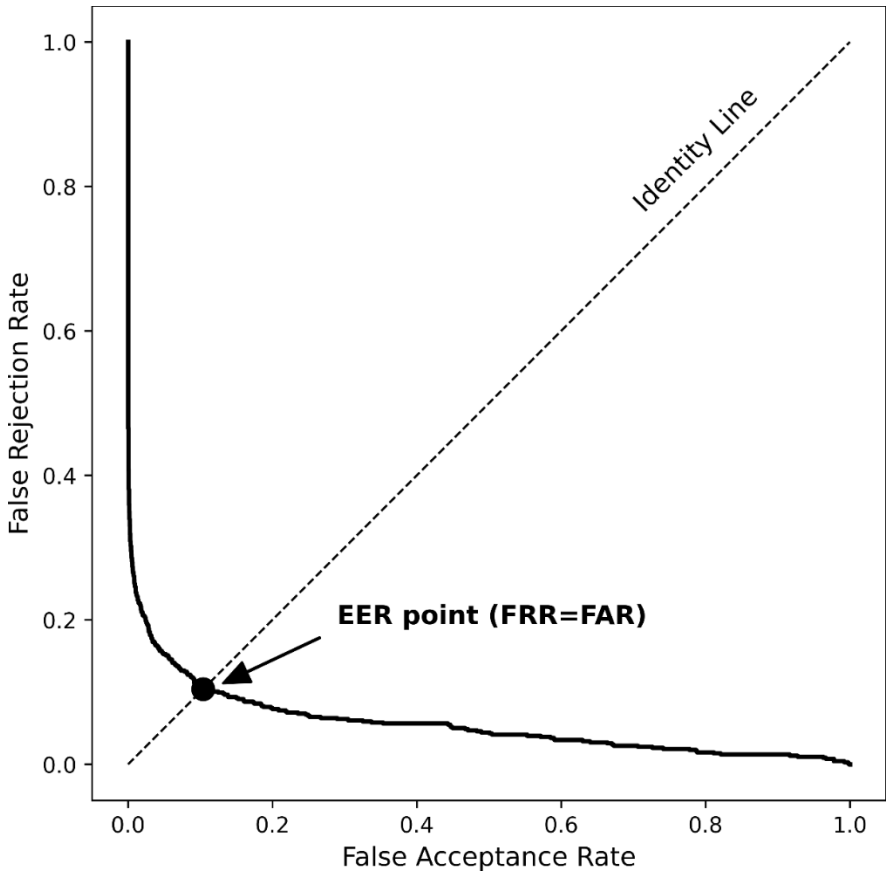

Figure 3.8. Detection error trade-off (DET) curve depicting the trade-off between FRR and FAR. The point on the curve where the FRR and FAR values are equal signifies the equal error rate (EER).

CHAPTER 4

RESULTS

4.1 Identification and Authentication Performance

We evaluated the identification and authentication performances for MCL, KFD and five common features. Identification was realized by assigning the observed data to the nearest existing class, while authentication was based upon deciding whether an observation belongs to a class or not, with respect to a distance threshold. A dimensionality reduction was incorporated into the classification pipeline for the features of PLV, COH and AR. The obtained performances per each feature are given in Table 4.1 in terms of the mean CRR ± the standard deviation of a 6-fold cross-validation for the identification and EER for the authentication tasks.

All features yielded comparably high identification performances of over 95 %. Specifically, a CRR of 99.4 ± 0.4 % in the EO condition and a slightly lower CRR of 98.8 ± 1.1 % in the EC condition were obtained for MCL, which were close to those obtained for KFD. In general, the EO condition facilitated better identification performances than the EC condition, which is in line with the literature (Demuru & Fraschini, 2020; Fraschini et al., 2014; Thomas & Vinod, 2016; Wang et al., 2019a).

Authentication performance was distinctively low only for the features of PSD and AP, with high EERs of more than 15 % (Fig. 4.1). For MCL, acceptable EERs of 6.29 % and 10.40 % were obtained, respectively for the EO and EC conditions.

The conspicuous difference of within-subject and between-subject variances for all channels exhibited in Fig. 4.2 verifies the high biometric performances achieved with MCL. The three highest ratios of between-subject variance to within-subject variance were observed at C_4, followed by FC_6 and F_6 channels in EO and TP_7, C_4

and T_7 channels in EC. Furthermore, a direct visualization of MCL feature vectors for six arbitrary subjects in Fig. 4.3 exhibits the unique correspondence of subjective brainwaves to the MCL prints, which are almost indistinguishable for the temporally different segments of the EEG signals.

Table 4.1 Identification and authentication performances of MCL and five other features in terms of CRR (mean ± standard deviation of 6-fold cross-validation) and ERR (corresponding to the DET curves in Fig. 4.1), respectively. Features marked by † were incorporated with a dimensionality reduction corresponding to a 99 % retained variance in their classification.

	Identification		**Authentication**	
Features	**EO CRR**	**EC CRR**	**EO ERR**	**EC ERR**
MCL	99.4 ± 0.4 %	98.8 ± 1.1 %	6.29 %	10.40 %
KFD	99.4 ± 0.7 %	98.9 ± 1.2 %	3.31 %	6.19 %
PSD (beta and gamma)	97.4 ± 1.4 %	95.9 ± 1.6 %	28.40 %	31.80 %
AP (exponent and offset)	99.2 ± 0.6 %	99.2 ± 0.6 %	18.33 %	15.07 %
PLV† (beta and gamma)	100.0 %	100.0 %	1.35 %	2.63 %
COH† (beta and gamma)	100.0 %	99.8 ± 0.3 %	2.98 %	1.10 %
AR† (5^{th} order)	97.9 ± 2.8 %	97.6 ± 1.9 %	6.11 %	5.33 %

Contrary to the comparable recognition performances among the features, there were substantial differences in the computational requirements (Table 4.2), particularly regarding the average runtimes (over subjects and conditions) during the feature extraction stage. MCL had the shortest runtime (0.03 s) and also the smallest feature vector size (64 feature elements, one per channel). Specifically, it was more than twice faster than KFD and two orders of magnitude faster than PLV and COH. Moreover, it has a linear computational complexity with respect to the number of channels, opposed to the quadratic complexity of the functional connectivity metrics.

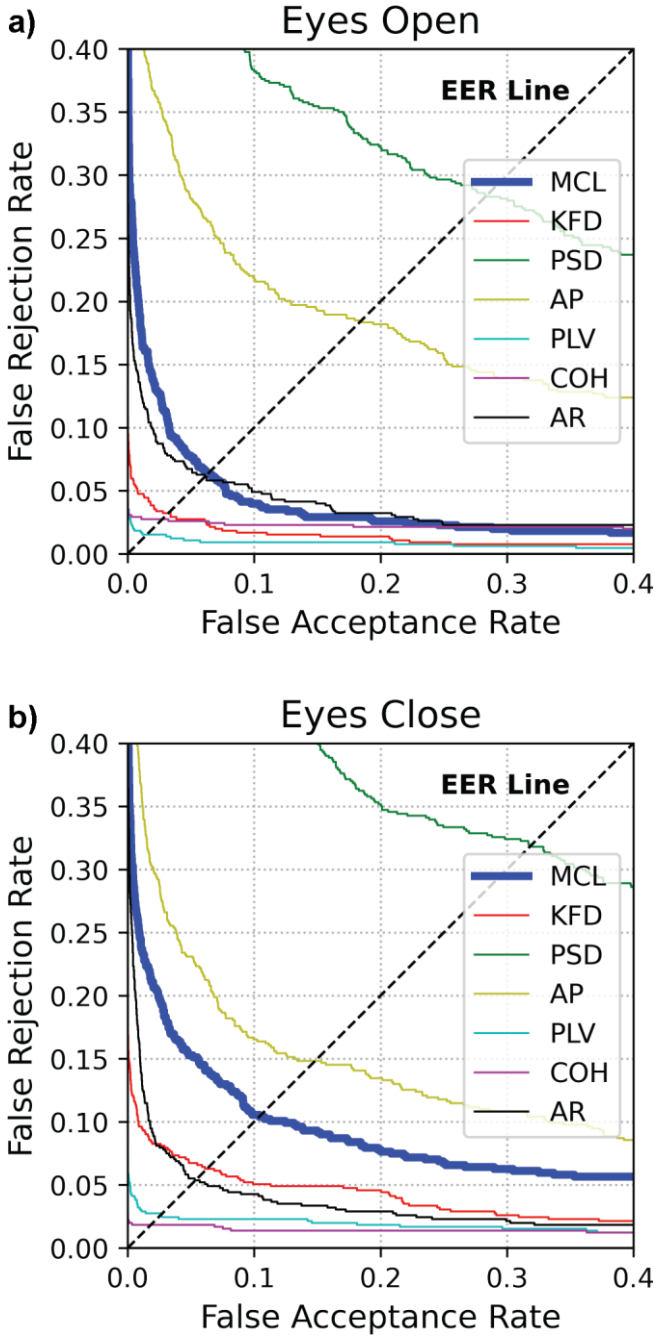

Figure 4.1. Detection error trade-off (DET) curves for all features in the authentication task. Mean curve length (bold blue curve) lies below PSD and AP, which indicates that it performed better than them in the authentication. It lies above KFD, PLV and COH, indicating a poorer performance relative to those. The intersection point between each curve and the EER identity line is the equal error rate of the corresponding feature.

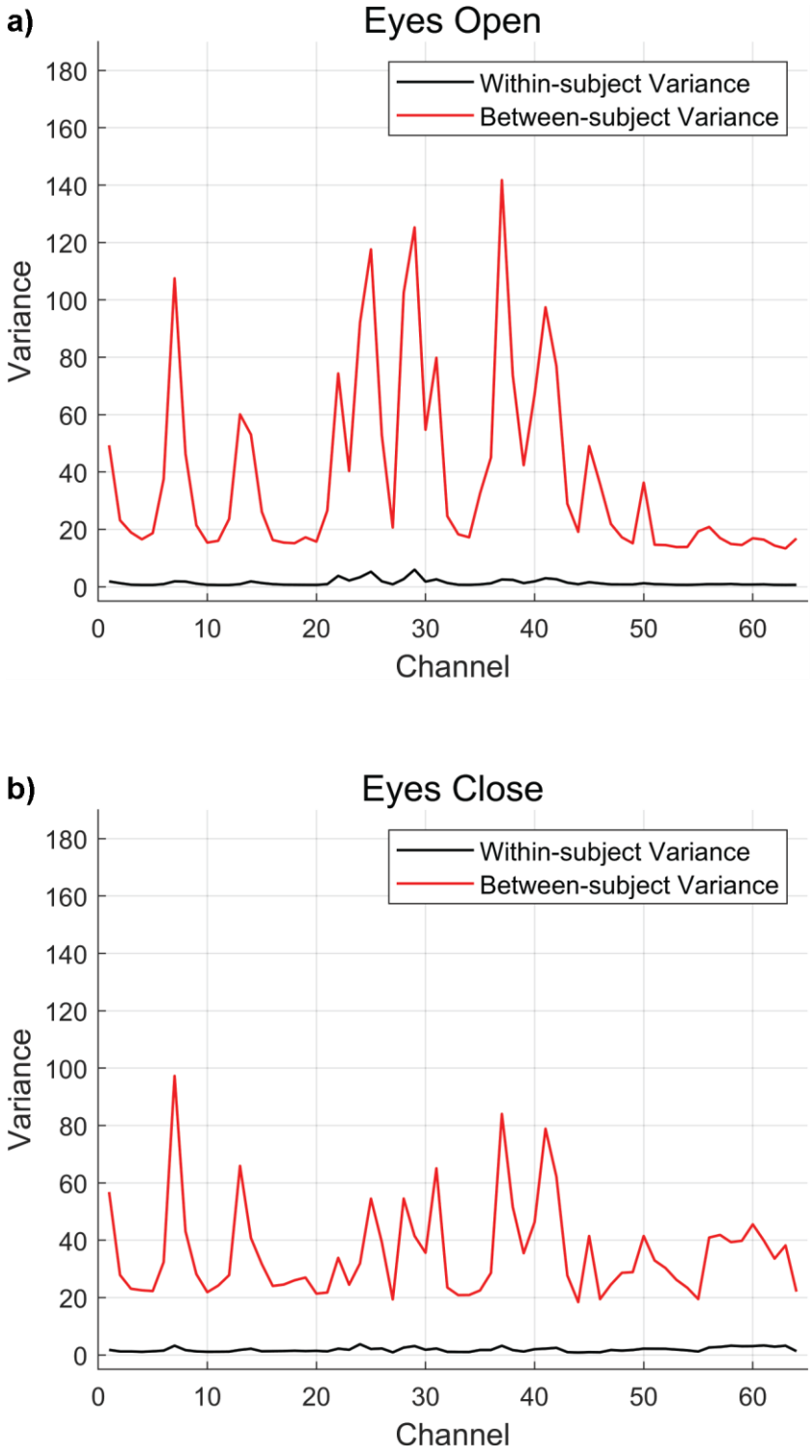

Figure 4.2. Within-subject (black) and between-subject (red) variances of MCL for all channels in the (a) EO and (b) EC conditions. Subject 79 in EO and subjects 21 & 103 in EC were excluded as outliers.

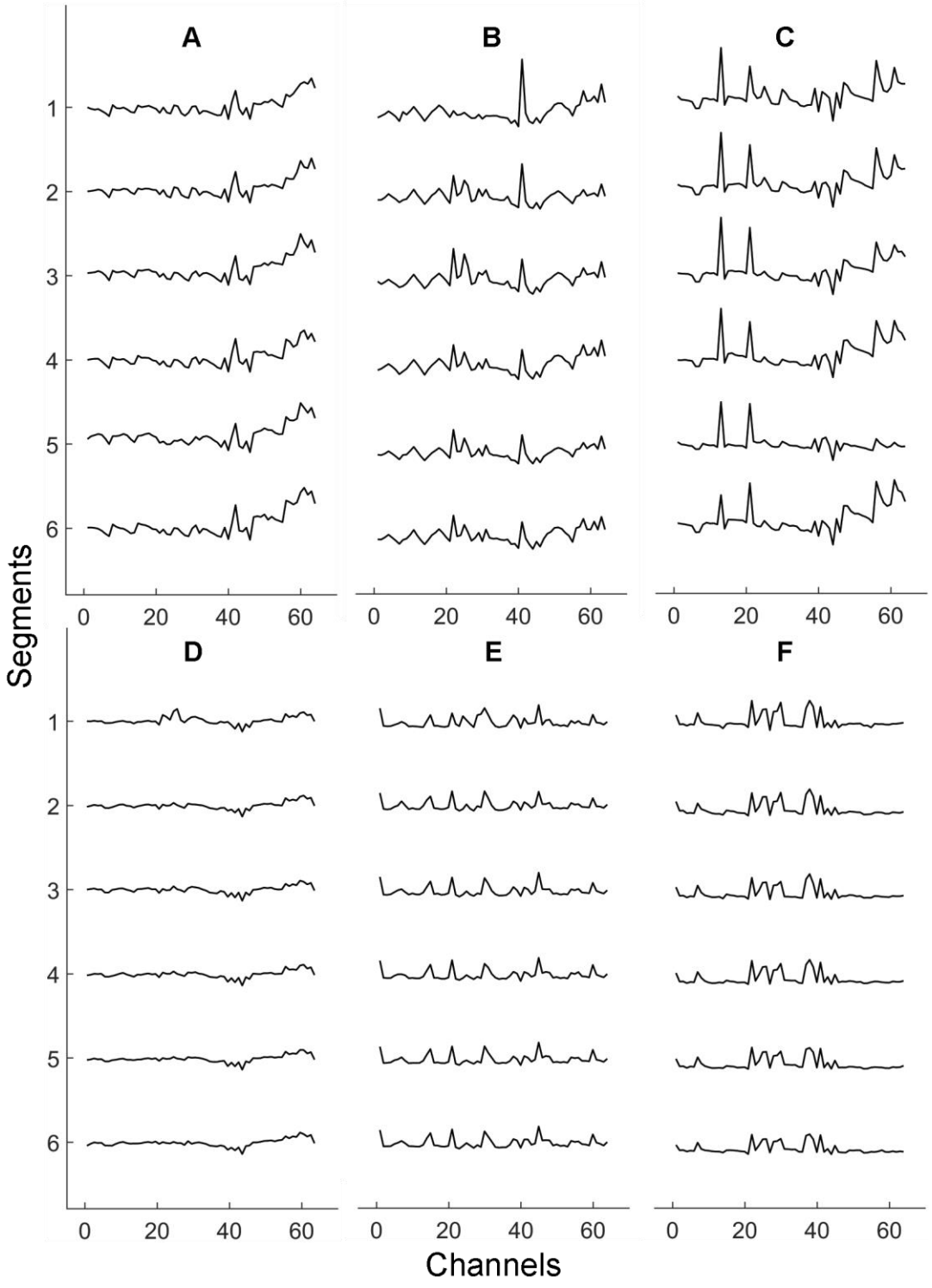

Figure 4.3. MCL feature vectors (corresponding to the features from 64 channels) of different temporal segments for six arbitrary subjects. The conspicuous similarity over time per each subject demonstrates MCL as a distinctive biometric feature.

Table 4.2 Computational complexities of MCL and other features in terms of feature vector size, average number of principal components over subjects and conditions (only for PLV, COH and AR), average runtime over subjects and conditions and analytical time complexity (e = # of channels, t = # of time points, p = order of the AR model). Features marked by † were incorporated with a dimensionality reduction corresponding to a 99 % retained variance in their classification.

Features	Feature Size (→ Average number of Principal Components)	Average Runtime	Time Complexity
MCL	64	0.03 s	$O(e \times t)$
KFD	64	0.07 s	$O(e \times t)$
PSD	64 × 2	0.29 s	$O(e \times t)$
AP	64 × 2	115.6 s	$O(e \times t^2)$
PLV†	(64 × 63 / 2) × 2 → 250 p.c.	2.30 s	$O(e^2 \times t)$
COH†	(64 × 63 / 2) × 2 → 163 p.c.	1.17 s	$O(e^2 \times t)$
AR†	64 × 5 → 56 p.c.	0.14 s	$O(e \times p \times t)$

4.2 Channel Contributions to Identification

We investigated channel contributions to the identification performance of MCL. Due to the volume conduction effect in the scalp EEG, a great overlap of signals occurs between channels, creating redundancy of information. Each channel is expected to contribute to the performance depending also on its correlation with the other channels. Therefore, ranking the classification performance of channels independently is not useful.

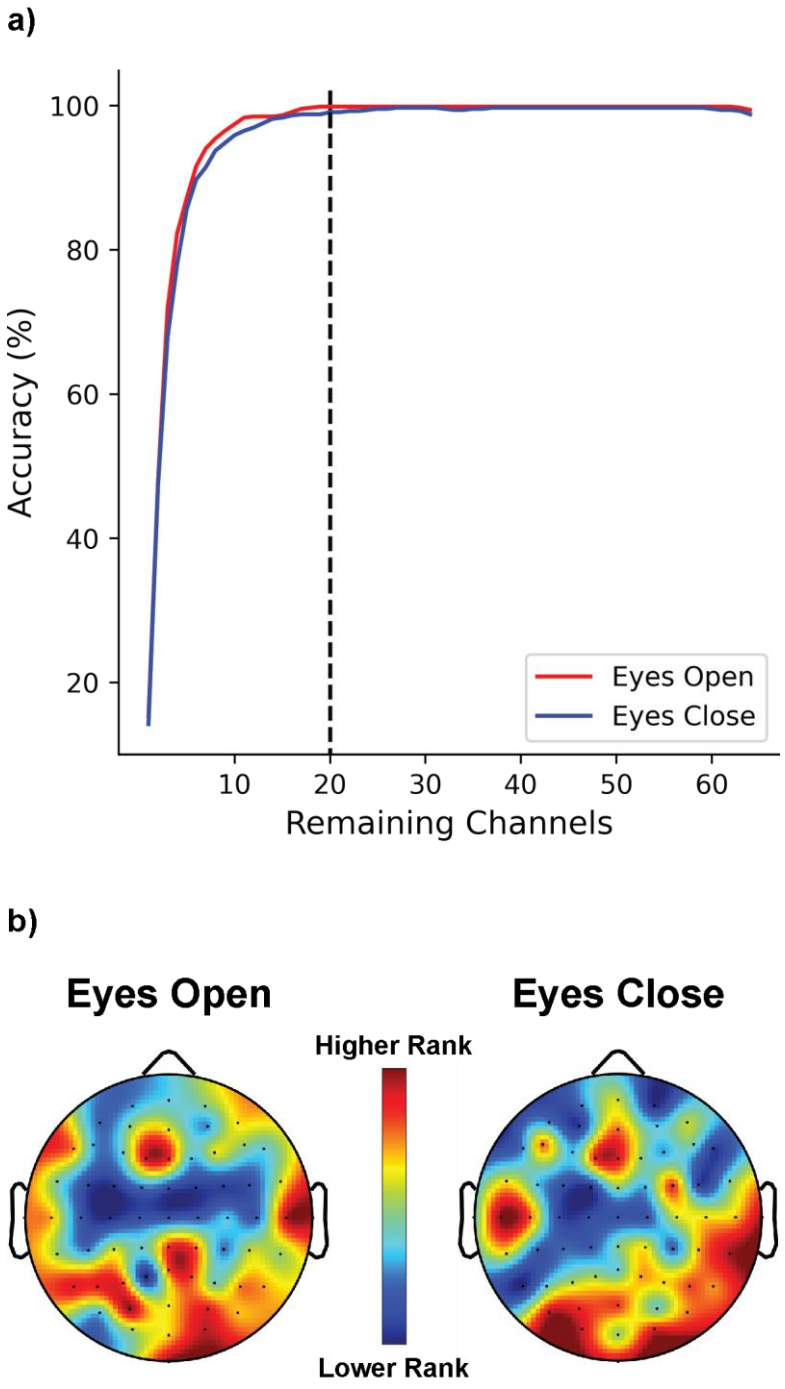

Figure 4.4. (a) The maximum cross-validated identification accuracy via recursive feature elimination (RFE) was reached with a minimum of 19 channels (99.8 %) and 27 channels (99.7 %) in the EO and EC conditions, respectively. (b) Topographical views of the channel ranks for the EO and EC conditions. The most discriminating features are at the parieto-occipital and temporal regions.

We adopted the so-called recursive feature elimination (RFE) method for ranking the channels based on their overall contribution to the identification performance. Starting with the set of all 64 channels, one channel was removed at each step, such that without that channel, the highest accuracy is obtained with the remaining channels. We observed that the identification accuracy for both conditions kept stable as long as the number of channels was about more than 20 (Fig. 4.4 (a)). The highest accuracies (even a bit more than the one using the full channel set) were achieved with a minimum of 19 channels in EO (99.8 %) and 27 channels in EC (99.7 %).

Channels were ranked according to their elimination step, e.g., the lowest rank of 1 was assigned to the first removed channel, while the last one standing had the highest rank of 64. The channel ranks are represented on the topographical maps in Fig. 4.4 (b). The highest ranks belonged to I_z, followed by PO_3 and T_{10} in EO and T_7, T_{10} and TP_8 in EC. The first three highest ranks appeared in both conditions belonged to T_{10}, I_z and O_2. In general, higher contributions mainly stemmed from the channels located at the parieto-occipital and temporal regions of the brain for both EO and EC conditions in accordance with the recent literature localizing the spectral neural fingerprints in source level (da Silva Castanheira et al., 2021).

4.3 Spectral MCL

Similar to extracting features such as power and functional connectivity from spectral band activities, it is possible to compute MCL from band-pass filtered signals. We performed person identification and authentication using spectral MCL features to determine whether there would be any increase in the performance relative to the broadband MCL. The five canonical frequency bands and the combination of beta and gamma bands were included in the analysis. The results indicated that the spectral MCL in all bands had in fact poorer performances in both identification and authentication relative to the broadband MCL (Table 4.3; Fig. 4.5). This shows that unlike power and functional connectivity measures (da Silva

Castanheira et al., 2021), extracting MCL from spectral bands does not increase the performance. Beta and gamma bands still outperformed the lower frequency bands, which further confirms the results of the previous literature outlined in Section 2.5. Their combination, however, performed worse than using them alone. The EO condition again facilitated a better performance than EC (Table 4.1, 4.3).

Table 4.3 Identification and authentication performances of spectral and broadband MCL features in terms of CRR (mean ± standard deviation of 6-fold cross-validation) and ERR (corresponding to the DET curve in Fig. 4.5), respectively.

	Identification		**Authentication**	
Features	**EO CRR**	**EC CRR**	**EO ERR**	**EC ERR**
Delta	75.7 ± 3.1 %	74.2 ± 6.0 %	30.27 %	31.98 %
Theta	85.8 ± 2.1 %	86.7 ± 3.0 %	28.44 %	29.98 %
Alpha	89.4 ± 3.4 %	90.4 ± 5.9 %	27.31 %	27.35 %
Beta	98.8 ± 0.7 %	95.1 ± 1.3 %	17.09 %	21.71 %
Gamma	95.1 ± 1.7 %	94.6 ± 1.8 %	14.92 %	19.53 %
Beta and gamma	97.4 ± 1.4 %	95.9 ± 1.6 %	28.40 %	31.80 %
Broadband	99.4 ± 0.4 %	98.8 ± 1.1 %	6.29 %	10.40 %

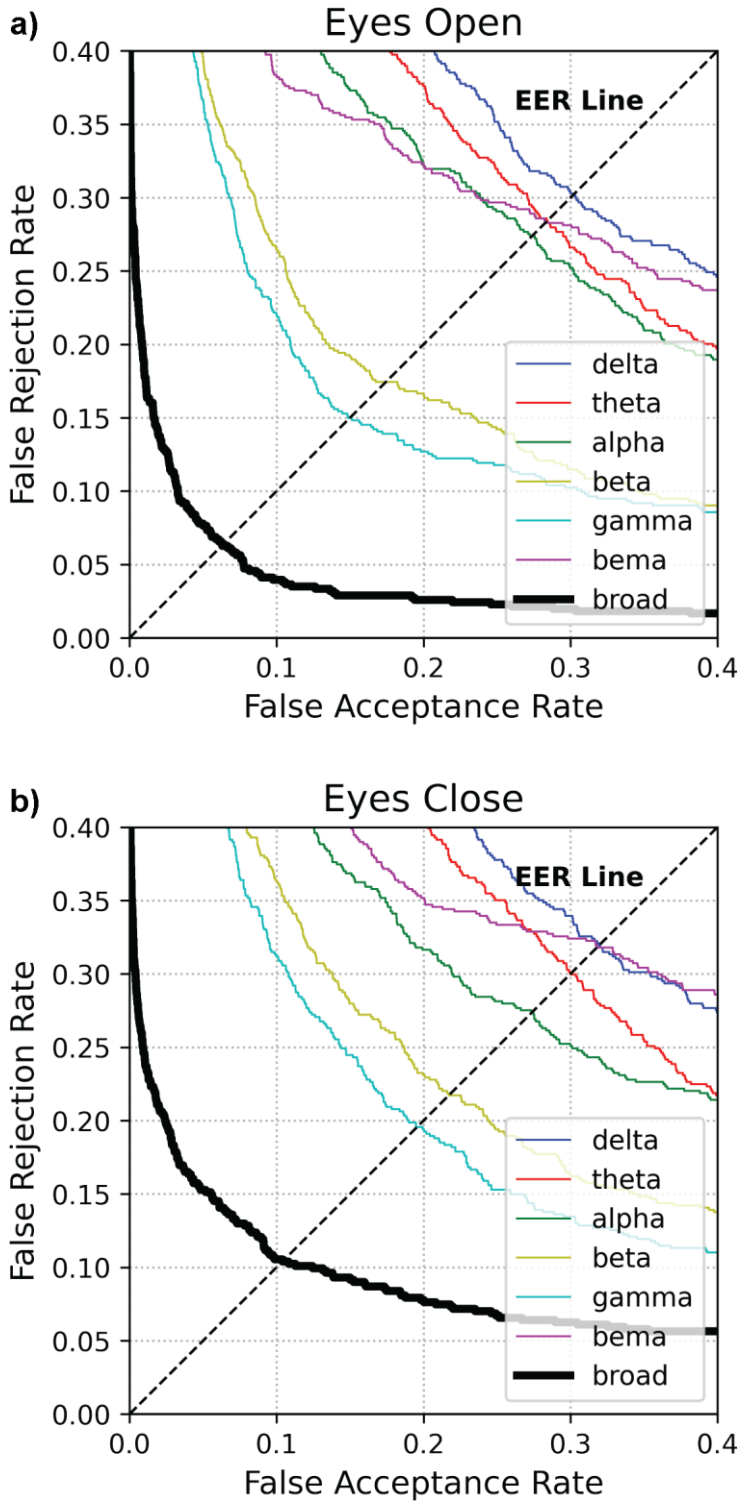

Figure 4.5. DET curves for the spectral and broadband MCL features in the authentication task. MCL from the original broadband signal (bold black curve) performed better than all spectral band MCLs. Bema abbreviates beta and gamma.

4.4 Effect of Using Mismatched Covariance Matrix

Retraining a Mahalanobis classifier consists in updating the covariance matrix and templates when users are needed to be either added to or removed from the database. We sought to investigate the degree of the importance of updating the covariance matrix in retraining. For this purpose, the robustness of the identification performance of MCL was questioned when a mismatched covariance matrix was employed for the classification.

We divided the 109 subjects randomly into two exclusive groups of unequal size: 20 (group I) and 89 (group II) subjects. Within each group, the subjects were classified in three ways: by computing the Mahalanobis distance (Eq. 3.13) using the covariance matrix of i) the group itself, ii) the other group and iii) using no covariance matrix, i.e., computing the Euclidean distance. The average classification mean and standard deviation were obtained for a total of 500 random subject splits (Table 4.4). Sample covariance matrices computed from random subsets of the subjects and the covariance matrix of the full set are provided in Appendix C for comparison.

We found out that using a mismatched covariance matrix still yielded a significantly higher performance in both groups and conditions than using plain Euclidean distance. The reduction in the identification performance was less in group I than group II, indicating that utilizing a larger population for estimating the covariance matrix mitigated the performance deterioration from the mismatch. Furthermore in the EC condition, a more robust estimation of the covariance matrix facilitated a better performance for group II than group I. This is despite that group II contained more subjects to classify, hence performed significantly worse than group I when plain Euclidean distance was used.

Table 4.4 Effect of using mismatched covariance matrices on MCL's identification performance. Generally, covariance matrix estimations from a greater number of samples and subjects (matched or not) are more robust and hence perform better. The results below are the average of 500 iterations of random selection.

EO			
	Group I Covariance Matrix	**Group II Covariance Matrix**	**No Covariance Matrix (Euclidean)**
Group I (20 subjects)	99.5 ± 1.0 %	99.3 ± 1.1 %	97.3 ± 2.6 %
Group II (89 subjects)	98.1 ± 1.1 %	99.3 ± 0.7 %	96.0 ± 1.6 %
EC			
	Group I Covariance Matrix	**Group II Covariance Matrix**	**No Covariance Matrix (Euclidean)**
Group I (20 subjects)	98.5 ± 2.0 %	97.9 ± 2.0 %	94.1 ± 4.0 %
Group II (89 subjects)	96.6 ± 1.3 %	98.7 ± 1.1 %	89.8 ± 3.0 %

CHAPTER 5

DISCUSSION AND CONCLUSION

5.1 Discussion

Our study demonstrated MCL as a comparably high performance, while vastly more efficient feature, compared to the other well-established and highly discriminative features that have been regularly employed in the state-of-the-art EEG-based biometric systems. The performance of MCL was further validated by showing that its between-subject variance is significantly higher than its within-subject variance. It is worthwhile to note that statistical measures of comparable simplicity, such as power and variance, do not provide the same level of individual distinction. Nonetheless, the recognition performance of EEG-based biometric systems have already reached a satisfactory level of more than 95 %. Thus, the focus is gradually shifting towards addressing other obstacles that hinder EEG from becoming an acceptable biometric modality. Despite the great progress in the computational power in the last decades, efficiency in computation and memory load still remains to be crucial for minimizing the delay in real-time biometric applications. Many state-of-the-art methods presented in the literature can simply be too complex and slow to be practically applied in continuous authentication systems. In this regard, the remarkable speed of computation grants MCL a unique advantage in real-world and real-time biometric systems such as mobile EEG.

It should be noted that in this study, we only tested the proposed feature without channel optimization, as we intended to compare it with the other features in a general way. Even though the feature vector size of MCL was already the smallest, it could have been further reduced by keeping only the channels that contain most of the discriminating information about the subjects. The RFE analysis revealed that

only a small subset of channels was enough for the identification task without compromising the performance. As a matter of fact, with less than half of the 64 channels, the system reached a higher accuracy than employing the full channel set. These channels were mainly located at the parieto-occipital and temporal regions.

In addition to its computational efficiency, the implementation of MCL is also immensely easier, without the requirement of any specialized programming libraries. This is in contrast to the reliance on band-pass filtering, data transformation, curve fitting and third-party functions to perform the sophisticated calculations in the case of PSD, AP, AR and functional connectivity matrices of PLV and COH. Moreover, there are no required parameters in the computation of MCL. Whereas for the other features, there exist numerous estimation methods, basis functions and other filtering parameters that affect the values of the resultant features. In addition to those parameters, there are multiple settings for curve fitting for AP and a model order parameter for AR. This makes MCL an attractive feature for a practitioner, since it does not need any consideration of a priori inputs to the system.

In our methodology, we performed a minimal preprocessing, only filtering out the high-frequency components of EEG signals beyond the conventional bands, which are mainly dominated by noise. Sophisticated artifact removal preprocessing may become counterproductive, since it distorts signal and reduces practicality in real-life applications. In fact, some artifacts may even be useful in individual discrimination. For example, volume conduction effect (Fraschini et al., 2018; La Rocca et al., 2014; Wang et al., 2021) and muscle activity in high-beta and gamma (> 20 Hz) (Fraschini et al., 2014) were found to be contributing to the subject classification performance.

In the classification stage, we took a template-based scheme and employed Mahalanobis distance as a measure of dissimilarity. Our results indicated that this simple approach provides satisfactory performance while having a lower computational complexity. In particular, the modified version of Mahalanobis classifier was shown to be an effective and much faster alternative to deep learning

(Wang et al., 2019a) and exhaustive feature selection (La Rocca et al., 2014) approaches for high-dimensional features. Retraining the classifier, when adding or removing a user, solely requires updating the covariance matrix, which is considerably cheaper (especially when the feature vector is small) than full retraining in the case of most other classifiers. Our analysis has revealed that as long as enough samples from many subjects are used for the estimation of the covariance matrix, regardless of being authorized users or not, the classification performance shall not significantly decrease.

5.2 Limitations and Future Studies

There is still room for improving MCL's performance by channel optimization or fusion with other efficient features that contain independent new information. Other topics for future studies are the permanence of MCL, its limitations as a univariate feature and solutions for it. Univariate features can easily be affected by the EEG amplitude changes due to the changes in signal acquisition conditions, therefore a normalization is possibly needed to immunize MCL against those.

Brainwaves can be affected by mental states, disease, medication, substance-use or simply as a result of aging (Chan et al., 2018). Thus in developing an EEG-based biometric system, considering these factors is important. The permanence of brain characteristics across time, in general, has not been extensively studied in the literature, since it requires longitudinal datasets of brain signals collected in multiple sessions, and these datasets are rare. Some studies on this issue have suggested the stability of EEG characteristics over the course of time, although, different features exhibited different levels of robustness in their biometric performance (da Silva Castanheira et al., 2021; Maiorana et al., 2015; Zhang et al., 2021). For example in da Silva Castanheira et al. (2021), 47 subjects were identified from within-session and between-session (201.7 days on average) EEG records using PSD and functional connectivity (FC) features. While PSD features were robust longitudinally (96.2 % to 97.9 %), the performance of FC features deteriorated from 94.9 % down to 89.4

%. A similar analysis can assess the longevity of MCL. Nevertheless, in a study of age-related changes in the EEG signal complexity represented by the fractal dimension (FD) (Zappasodi et al., 2015), it was found that FD of resting state EEG followed an inverted-U-shape across the ages in 40 healthy subjects, increasing from late-adolescence (FD: 1.41 ± 0.07, age: 20.6 ± 2.1 years) towards adulthood (FD: 1.53 ±0.08, age: 41.1 ± 15.4 years) and decreasing during old age (FD: 1.48 ± 0.12, age: 73.6 ± 4.8 years). Since MCL is strongly correlated with the Katz Fractal dimension, it may follow a similar pattern. However, it is important to note that these changes may occur over a much longer time interval than a typical multi-session biometric study.

A number of countermeasures have been proposed by Chan et al. (2018) and Maiorana and Campisi (2017) to tackle the longitudinal within-subject variations of EEG across time span. Regularly updating the biometric system using newly registered user data is one of the commonly used strategies to reduce the time effect on the recognition performance (Didaci et al., 2014). Another set of solutions include fusing data at different levels (feature level, score level and decision level) for classification, where different EEG features and features corresponding to different mental conditions can be fused together. According to Maiorana and Campisi (2017), the fusion strategy "exploits the heterogeneity of aging effects on different biometric representations to limit their impact on the achievable verification accuracy." Furthermore, Chan et al. (2018) proposed a multimodal fusion of EEG-based biometrics with other biometric modalities in order to mutually compensate for each other's weaknesses. They also proposed dataset augmentation by modeling the changes in EEG features caused by psychological and physiological factors.

5.3 Conclusion

Neural fingerprints do not need to be obtained solely through conventional spectral band activities or functional connectivity metrics. In this study, we proposed and demonstrated the effectiveness of mean curve length as a promising feature for EEG-

based biometric identification and authentication. Despite its simplicity, MCL provides a remarkably unique characterization of individual brainwaves. The order of magnitude increase in the speed together with its simplicity of formulation endows MCL with a powerful efficiency and capability desirable for real-time continuous brain biometrics. Our study signifies the potential usefulness of measures other than those derived from conventional EEG band activities and their functional interrelations, and it further promotes fractal-based analyses of brain dynamics, especially by acknowledging that brainwaves are representations of a complex system.

REFERENCES

Akgül, T., Sun, M., Sclabassi, R. J., & Çetin, A. E. (2000). Characterization of sleep spindles using higher order statistics and spectra. *IEEE Transactions on Biomedical Engineering*, *47*(8), 997-1009.

Alzahab, N. A., Baldi, M., & Scalise, L. (2021, June). Efficient feature selection for electroencephalogram-based authentication. *IEEE International Symposium on Medical Measurements and Applications (MeMeA)* (pp. 1-6). IEEE.

Bidgoly, A. J., Bidgoly, H. J., & Arezoumand, Z. (2020). A survey on methods and challenges in EEG based authentication. *Computers & Security*, *93*, 101788.

Blum, S., Debener, S., Emkes, R., Volkening, N., Fudickar, S., & Bleichner, M. G. (2017). EEG recording and online signal processing on android: A multiapp framework for brain-computer interfaces on smartphone. *BioMed research international*.

Bos, R., De Waele, S., & Broersen, P. M. (2002). Autoregressive spectral estimation by application of the Burg algorithm to irregularly sampled data. *IEEE Transactions on Instrumentation and Measurement*, *51*(6), 1289-1294.

Boulay, C., Stenner, T., & Medine, D. (n.d.). *Lab streaming layer (LSL)*. GitHub. https://github.com/sccn/labstreaminglayer

Campisi, P., & La Rocca, D. (2014). Brain waves for automatic biometric-based user recognition. *IEEE transactions on information forensics and security*, *9*(5), 782-800.

Casson, A. J. (2019). Wearable EEG and beyond. *Biomedical engineering letters*, *9*(1), 53-71.

Chan, H. L., Kuo, P. C., Cheng, C. Y., & Chen, Y. S. (2018). Challenges and future perspectives on electroencephalogram-based biometrics in person recognition. *Frontiers in neuroinformatics*, 66.

Chen, J., Benesty, J., & Huang, Y. A. (2005). Performance of GCC-and AMDF-based time-delay estimation in practical reverberant environments. *EURASIP Journal on Advances in Signal Processing* (1), 1-12.

Claus, S., Velis, D., da Silva, F. H. L., Viergever, M. A., & Kalitzin, S. (2012). High frequency spectral components after secobarbital: the contribution of muscular origin—a study with MEG/EEG. *Epilepsy research*, *100*(1-2), 132-141.

Cohen, M. X. (2014). *Analyzing neural time series data: theory and practice*. MIT press.

da Silva Castanheira, J., Orozco Perez, H. D., Misic, B., & Baillet, S. (2021). Brief segments of neurophysiological activity enable individual differentiation. *Nature communications*, *12*(1), 1-11.

Das, B. B., Kumar, P., Kar, D., Ram, S. K., Babu, K. S., & Mohapatra, R. K. (2019). A spatio-temporal model for EEG-based person identification. *Multimedia Tools and Applications*, *78*(19), 28157-28177.

DelPozo-Banos, M., Travieso, C. M., Ticay-Rivas, J. R., Alonso, J. B., Dutta, M. K., & Singh, A. (2015, August). Real cepstrums on electroencephalogram biometric identification. *Eighth International Conference on Contemporary Computing (IC3)* (pp. 54-58). IEEE.

Demuru, M., & Fraschini, M. (2020). EEG fingerprinting: Subject-specific signature based on the aperiodic component of power spectrum. *Computers in Biology and Medicine*, *120*, 103748.

Didaci, L., Marcialis, G. L., & Roli, F. (2014). Analysis of unsupervised template update in biometric recognition systems. *Pattern Recognition Letters*, *37*, 151-160.

Donoghue, T., Haller, M., Peterson, E. J., Varma, P., Sebastian, P., Gao, R., Noto, T., Lara, A. H., Wallis, J. D., Knight, R. T., Shestyuk, A., & Voytek, B. (2020). Parameterizing neural power spectra into periodic and aperiodic components. *Nature Neuroscience*, *23*(12), 1655–1665. https://doi.org/10.1038/s41593-020-00744-x

Dubuc, B., Quiniou, J. F., Roques-Carmes, C., Tricot, C., & Zucker, S. W. (1989). Evaluating the fractal dimension of profiles. *Physical Review A*, *39*(3), 1500.

Esteller, R., Echauz, J., Tcheng, T., Litt, B., & Pless, B. (2001, October). Line length: an efficient feature for seizure onset detection. *Conference Proceedings of the 23rd Annual International Conference of the IEEE Engineering in Medicine and Biology Society* (Vol. 2, pp. 1707-1710). IEEE.

Fraschini, M., Didaci, L., & Marcialis, G. L. (2018). EEG-based personal identification: comparison of different functional connectivity metrics. *bioRxiv*, 254557.

Fraschini, M., Hillebrand, A., Demuru, M., Didaci, L., & Marcialis, G. L. (2014). An EEG-based biometric system using eigenvector centrality in resting state brain networks. *IEEE Signal Processing Letters*, *22*(6), 666-670.

Goldberger, A. L., Amaral, L. A., Glass, L., Hausdorff, J. M., Ivanov, P. C., Mark, R. G., ... & Stanley, H. E. (2000). PhysioBank, PhysioToolkit, and PhysioNet: components of a new research resource for complex physiologic signals. *Circulation*, *101*(23), e215-e220.

Goncharova, I. I., McFarland, D. J., Vaughan, T. M., & Wolpaw, J. R. (2003). EMG contamination of EEG: spectral and topographical characteristics. *Clinical neurophysiology*, *114*(9), 1580-1593.

Gui, Q., Ruiz-Blondet, M. V., Laszlo, S., & Jin, Z. (2019). A survey on brain biometrics. *ACM Computing Surveys (CSUR)*, *51*(6), 1-38.

Gwin, J. T., Gramann, K., Makeig, S., & Ferris, D. P. (2011). Electrocortical activity is coupled to gait cycle phase during treadmill walking. *Neuroimage*, *54*(2), 1289-1296.

He, B. J. (2014). Scale-free brain activity: past, present, and future. *Trends in cognitive sciences*, *18*(9), 480-487.

Higuchi, T. (1988). Approach to an irregular time series on the basis of the fractal theory. *Physica D: Nonlinear Phenomena*, *31*(2), 277-283.

Hinkel, K. M., & Outcalt, S. I. (1995). Detection of heat-mass transfer regime transitions in the active layer using fractal geometric parameters. *Cold regions science and technology*, *23*(4), 293-304.

Hui, L., Dai, B. Q., & Wei, L. (2006, May). A pitch detection algorithm based on AMDF and ACF. *IEEE International Conference on Acoustics Speech and Signal Processing Proceedings* (Vol. 1, pp. I-I). IEEE.

Hurst, H. E. (1951). Long-term storage capacity of reservoirs. *Transactions of the American society of civil engineers*, *116*(1), 770-799.

IMEC. (n.d.). *Dry EEG electrodes*. https://www.imec-int.com/en/connected-health-solutions/dry-eeg-electrodes

Jain, A. K., Ross, A., & Prabhakar, S. (2004). An introduction to biometric recognition. *IEEE Transactions on circuits and systems for video technology*, *14*(1), 4-20.

Jijomon, C. M., & Vinod, A. P. (2018, December). EEG-based biometric identification using frequently occurring maximum power spectral features. *IEEE Applied Signal Processing Conference (ASPCON)* (pp. 249-252). IEEE.

Jung, R., & Berger, W. (1979). Hans bergers entdeckung des elektrenkephalogramms und seine ersten befunde 1924–1931. *Archiv für Psychiatrie und Nervenkrankheiten*, *227*(4), 279-300.

Katz, M. J. (1988). Fractals and the analysis of waveforms. *Computers in biology and medicine*, *18*(3), 145-156.

Keshishzadeh, S., Fallah, A., & Rashidi, S. (2016, May). Improved EEG based human authentication system on large dataset. *24th Iranian Conference on Electrical Engineering (ICEE)* (pp. 1165-1169). IEEE.

Kessy, A., Lewin, A., & Strimmer, K. (2018). Optimal whitening and decorrelation. *The American Statistician*, *72*(4), 309-314.

Kohli, S., & Casson, A. J. (2015, August). Towards out-of-the-lab EEG in uncontrolled environments: feasibility study of dry EEG recordings during exercise bike riding. *37th Annual International Conference of the IEEE Engineering in Medicine and Biology Society (EMBC)* (pp. 1025-1028). IEEE.

Kong, W., Wang, L., Xu, S., Babiloni, F., & Chen, H. (2019). EEG fingerprints: phase synchronization of EEG signals as biomarker for subject identification. *IEEE Access*, *7*, 121165-121173.

La Rocca, D., Campisi, P., & Scarano, G. (2013, February). On the Repeatability of EEG Features in a Biometric Recognition Framework using a Resting State Protocol. *BIOSIGNALS* (pp. 419-428).

La Rocca, D., Campisi, P., Vegso, B., Cserti, P., Kozmann, G., Babiloni, F., & Fallani, F. D. V. (2014). Human brain distinctiveness based on EEG spectral coherence connectivity. *IEEE transactions on Biomedical Engineering*, *61*(9), 2406-2412.

Lachaux, J. P., Rodriguez, E., Martinerie, J., & Varela, F. J. (1999). Measuring phase synchrony in brain signals. *Human brain mapping*, *8*(4), 194-208.

Lai, C. Q., Ibrahim, H., Abdullah, M. Z., Abdullah, J. M., Suandi, S. A., & Azman, A. (2019). Arrangements of resting state electroencephalography as the input to convolutional neural network for biometric identification. *Computational intelligence and neuroscience*.

Ma, L., Minett, J. W., Blu, T., & Wang, W. S. (2015, August). Resting state EEG-based biometrics for individual identification using convolutional neural networks. *37th Annual International Conference of the IEEE Engineering in Medicine and Biology Society (EMBC)* (pp. 2848-2851). IEEE.

Maiorana, E., & Campisi, P. (2017). Longitudinal evaluation of EEG-based biometric recognition. *IEEE transactions on Information Forensics and Security*, *13*(5), 1123-1138.

Maiorana, E., La Rocca, D., & Campisi, P. (2015). On the permanence of EEG signals for biometric recognition. *IEEE Transactions on Information Forensics and Security*, *11*(1), 163-175.

Malafeev, A. (2018). *Automatic Sleep Classification with Machine Learning* (Doctoral dissertation, University of Zurich).

Malmivuo, J. (2012). Comparison of the properties of EEG and MEG in detecting the electric activity of the brain. *Brain topography*, *25*(1), 1-19.

Mandelbrot, B. (1967). How long is the coast of Britain? Statistical self-similarity and fractional dimension. *Science*, *156*(3775), 636-638.

Millett, D. (2001). Hans Berger: From psychic energy to the EEG. *Perspectives in biology and medicine*, *44*(4), 522-542.

Moctezuma, L. A., & Molinas, M. (2019, July). Event-related potential from EEG for a two-step identity authentication system. *IEEE 17th International Conference on Industrial Informatics (INDIN)* (Vol. 1, pp. 392-399). IEEE.

Monge-Álvarez, J. (2021). *Higuchi and Katz fractal dimension measures*. MathWorks. https://www.mathworks.com/matlabcentral/fileexchange/50290-higuchi-and-katz-fractal-dimension-measures

Monsy, J. C., & Vinod, A. P. (2020). EEG-based biometric identification using frequency-weighted power feature. *IET Biometrics*, *9*(6), 251-258.

Mu, Z., Hu, J., & Min, J. (2016). EEG-based person authentication using a fuzzy entropy-related approach with two electrodes. *Entropy*, *18*(12), 432.

Mukai, K., & Nakanishi, I. (2020, November). Introduction of Fractal Dimension Feature and Reduction of Calculation Amount in Person Authentication Using Evoked EEG by Ultrasound. *IEEE REGION 10 CONFERENCE (TENCON)* (pp. 567-572). IEEE.

Özkurt, T. E., Akram, H., Zrinzo, L., Limousin, P., Foltynie, T., Oswal, A., & Litvak, V. (2020). Identification of nonlinear features in cortical and subcortical signals of Parkinson's Disease patients via a novel efficient measure. *NeuroImage*, *223*, 117356.

Özkurt, T. E., Sun, M., Akgül, T., & Sclabassi, R. J. (2006). Optimal feature selection for seizure detection: A subspace based approach. *International Conference of the IEEE Engineering in Medicine and Biology Society* (pp. 2134-2137). IEEE.

Peitgen, H. O., Jürgens, H., Saupe, D., Maletsky, E., Perciante, T., & Yunker, L. (1991). Self-Similarity. *Fractals for the Classroom: Strategic Activities Volume One* (pp. 1-36). Springer, New York, NY.

PhysioNet. (2009). *EEG motor movement/imagery dataset*. https://physionet.org/content/eegmmidb/1.0.0/

Pilgrim, I., & Taylor, R. P. (2018). Fractal analysis of time-series data sets: Methods and challenges. *Fractal analysis*.

Riley, M. A., Bonnette, S., Kuznetsov, N., Wallot, S., & Gao, J. (2012). A tutorial introduction to adaptive fractal analysis. *Frontiers in physiology*, *3*, 371.

Schons, T., Moreira, G. J., Silva, P. H., Coelho, V. N., & Luz, E. J. (2017). Convolutional network for EEG-based biometric. *Iberoamerican Congress on Pattern Recognition* (pp. 601-608). Springer, Cham.

Singh, B., Mishra, S., & Tiwary, U. S. (2015). EEG based biometric identification with reduced number of channels. *17th International Conference on Advanced Communication Technology (ICACT)* (pp. 687-691). IEEE.

Sun, Y., Lo, F. P. W., & Lo, B. (2019). EEG-based user identification system using 1D-convolutional long short-term memory neural networks. *Expert Systems with Applications*, *125*, 259-267.

Thomas, K. P., & Vinod, A. P. (2016). Biometric identification of persons using sample entropy features of EEG during rest state. *IEEE International Conference on Systems, Man, and Cybernetics (SMC)* (pp. 003487-003492). IEEE.

Thomas, K. P., & Vinod, A. P. (2018). EEG-based biometric authentication using gamma band power during rest state. *Circuits, Systems, and Signal Processing*, *37*(1), 277-289.

Vallat, R., & Van Der Donckt, J. (2021). *Fractal functions*. GitHub. https://github.com/raphaelvallat/antropy/blob/master/antropy/fractal.py

Wagner, J., Solis-Escalante, T., Grieshofer, P., Neuper, C., Müller-Putz, G., & Scherer, R. (2012). Level of participation in robotic-assisted treadmill walking modulates midline sensorimotor EEG rhythms in able-bodied subjects. *Neuroimage*, *63*(3), 1203-1211.

Walters-Williams, J., & Li, Y. (2010). Comparative study of distance functions for nearest neighbors. *Advanced techniques in computing sciences and software engineering* (pp. 79-84). Springer, Dordrecht.

Wang, M., El-Fiqi, H., Hu, J., & Abbass, H. A. (2019a). Convolutional neural networks using dynamic functional connectivity for EEG-based person identification in diverse human states. *IEEE Transactions on Information Forensics and Security*, *14*(12), 3259-3272.

Wang, M., Hu, J., & Abbass, H. A. (2019b). Stable EEG Biometrics Using Convolutional Neural Networks and Functional Connectivity. *Aust. J. Intell. Inf. Process. Syst.*, *15*(3), 19-26.

Wang, M., Hu, J., & Abbass, H. A. (2020). BrainPrint: EEG biometric identification based on analyzing brain connectivity graphs. *Pattern Recognition*, *105*, 107381.

Wang, M., Kasmarik, K., Bezerianos, A., Tan, K. C., & Abbass, H. (2021). On the channel density of EEG signals for reliable biometric recognition. *Pattern Recognition Letters*, *147*, 134-141.

Yang, S., Deravi, F., & Hoque, S. (2018). Task sensitivity in EEG biometric recognition. *Pattern Analysis and Applications*, *21*(1), 105-117.

Zappasodi, F., Marzetti, L., Olejarczyk, E., Tecchio, F., & Pizzella, V. (2015). Age-related changes in electroencephalographic signal complexity. *PloS one*, *10*(11), e0141995.

Zhang, Y., Li, M., Shen, H., & Hu, D. (2021). On the Specificity and Permanence of Electroencephalography Functional Connectivity. *Brain Sciences*, *11*(10), 1266.

Zink, R., Hunyadi, B., Van Huffel, S., & De Vos, M. (2016). Mobile EEG on the bike: disentangling attentional and physical contributions to auditory attention tasks. *Journal of neural engineering*, *13*(4), 046017.

APPENDICES

A. Effect of the Unit of Time on a Signal's Fractal Dimension

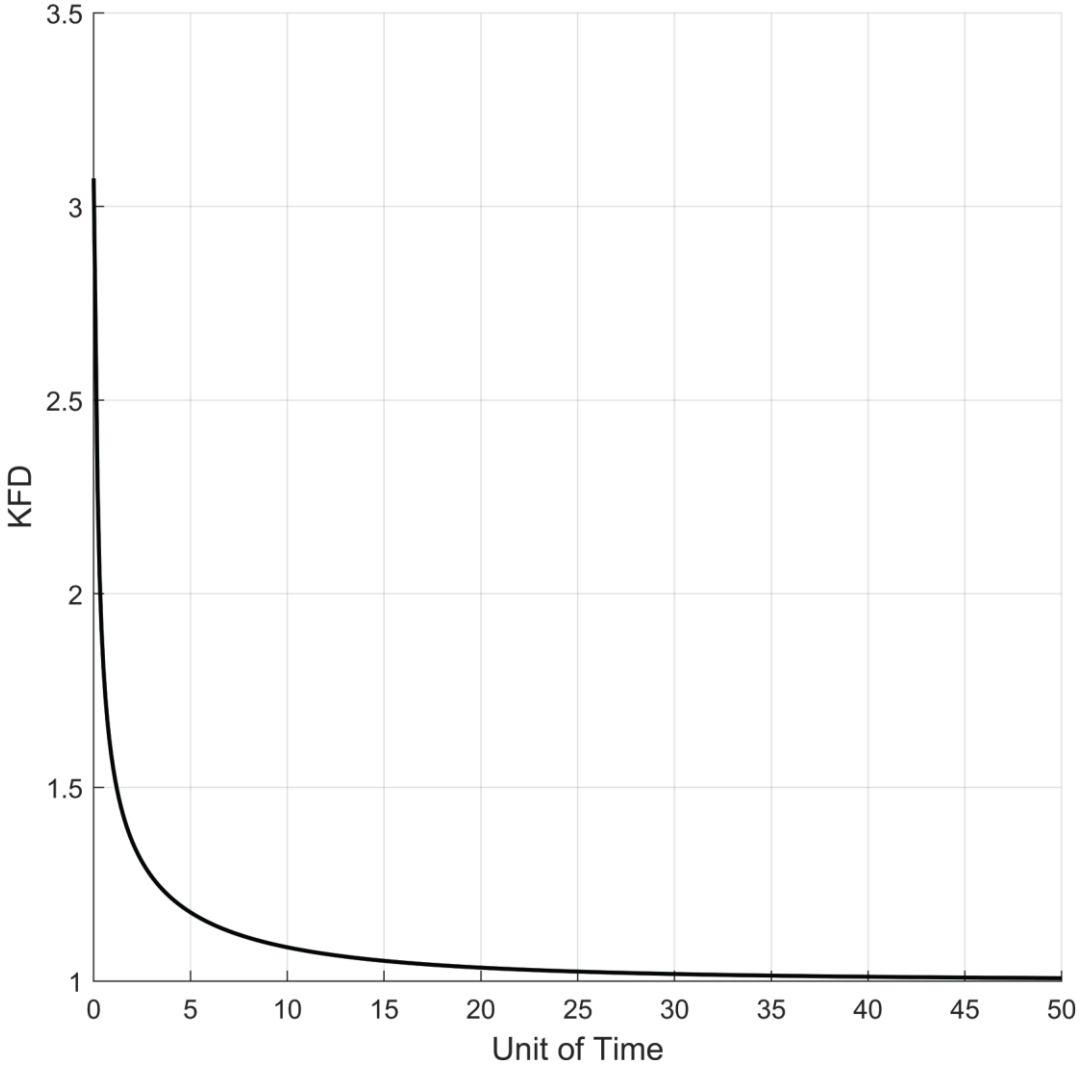

Figure A.1. Fractal dimension of an EEG signal as a function of the unit of time. By increasing the scale of the time-axis, the signal stretches towards a straight line, making its fractal dimension approach towards one.

B. Correlation Between MCL and KFD

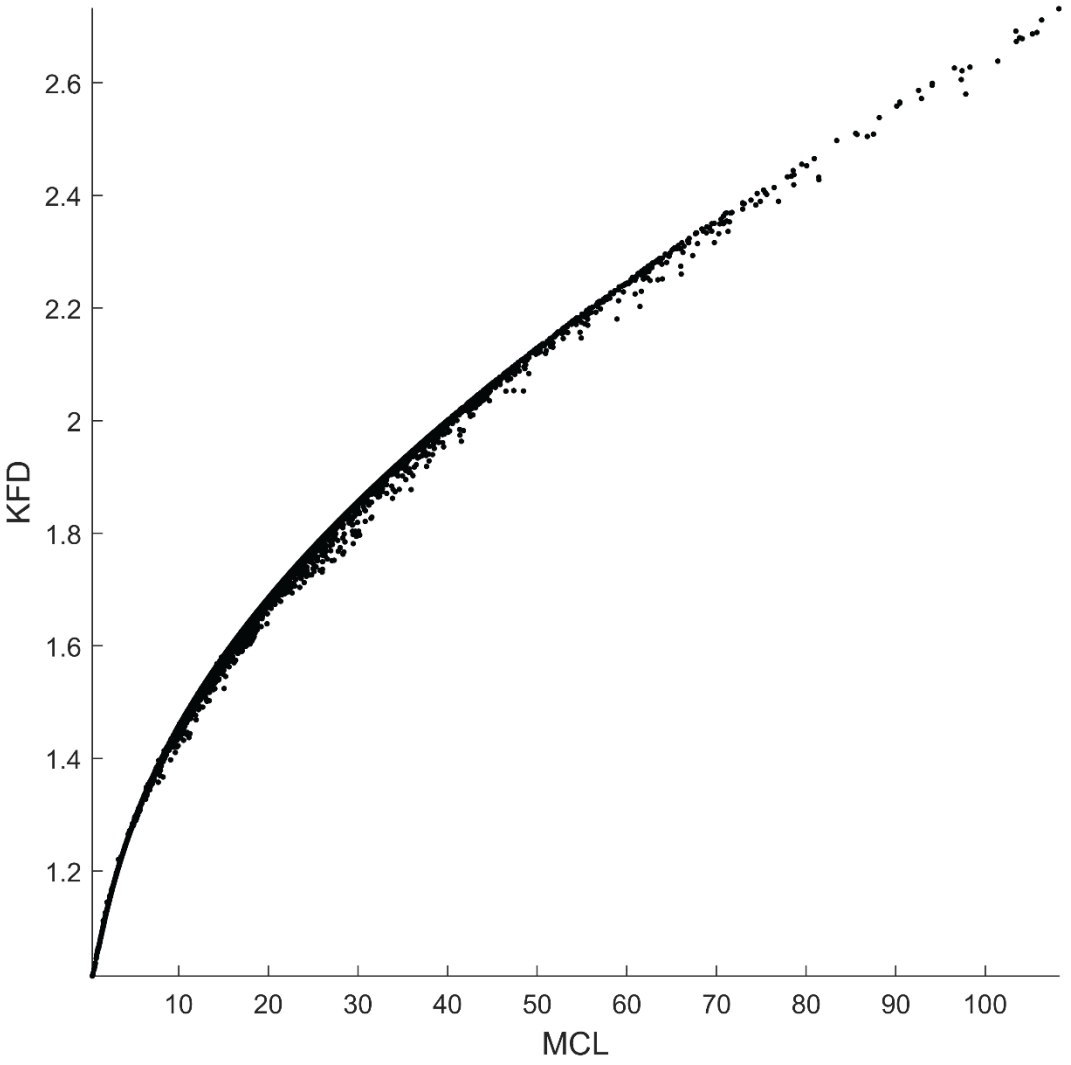

Figure B.1. KFD as a function of MCL, exhibiting the high correlation between them (r = 0.96, $p < 10^{-15}$). Samples (109×6×64) were pooled from all subjects, segments and channels.

C. Comparison Between Covariance Matrices from Random Subsets of Subjects and All Subjects

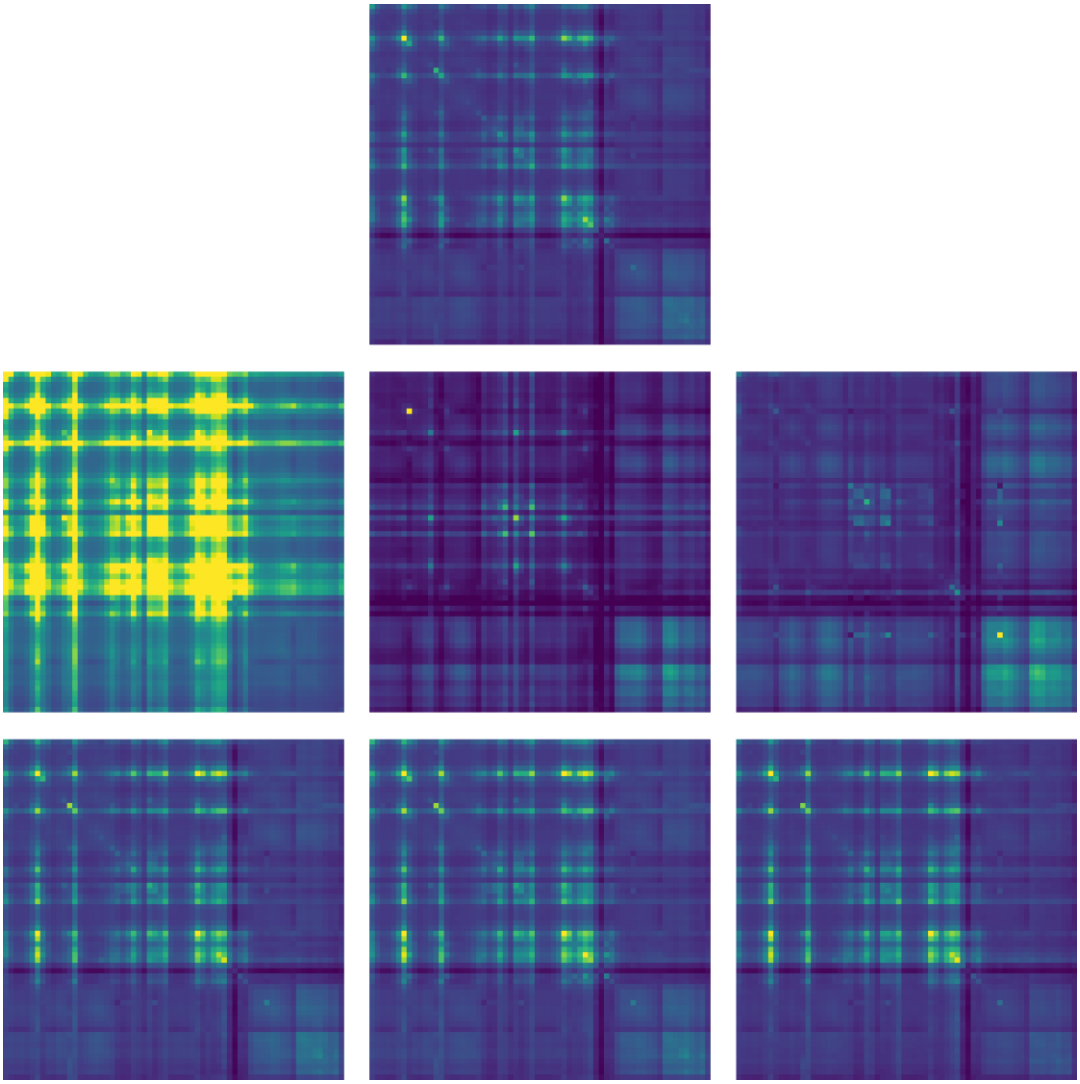

Figure C.1. Covariance matrix of all subjects (top), covariance matrices of 20 randomly selected (second row) and 80 randomly selected subjects (third row).